Improvement of the depolluting and self-cleaning abilities of air lime mortars with dispersing admixtures

J.F. González-Sánchez[a], B. Taşcı[b], J.M. Fernández[a], Í. Navarro-Blasco[a], J.I. Alvarez[a*]

[a] *Materials and Cultural Heritage, MATCH, Research Group, Department of Chemistry, University of Navarra, 31008 Pamplona, Spain*
[b] *Deparment of Architecture, Izmir Katip Çelebi University, 35620 Izmir, Turkey*

Published in **Journal of Cleaner Production 2021,** https://doi.org/10.1016/j.jclepro.2021.126069

Abstract

The aim of this study is to develop new air lime mortars with enhanced photocatalytic depolluting and self-cleaning abilities. Nanosilica, as pozzolanic mineral admixture, was used to improve the strength of mortars, whereas nanotitania (TiO_2) was added to impart photocatalytic properties. At the same time, five different dispersing admixtures –superplasticizers– were added in bulk to the mortars to enhance the photocatalytic activity by reducing the rate of charge carrier recombination. Four polycarboxylate-based derivatives and a polynaphthalene sulfonate were tested aiming to achieve an efficient charge separation. In order to increase the lasting of the mortars subjected to water movements, sodium oleate was also added as a water repellent agent. Since the photoinduced hydrophilicity, responsible for the self-cleaning effect, might be affected by the water repellent, the compatibility between this admixture and the photocatalytic performance of the nanotitania was also investigated. Results showed that photocatalytic activity was improved due to the action of the superplasticizers as indicated by an average 33% increase of NO degradation, which is significant to the depolluting activity of these mortars. Furthermore, these mortars also showed a greatly reduced release of intermediate toxic compounds, mainly NO_2: the selectivity factor (NO_x/NO) reached values up to 87%. The self-cleaning ability, studied through dye degradation, of the mortars with SPs was also enhanced around 1.2 times. Three of the polycarboxylate-based superplasticizers enhanced the photosensitization of the dye under visible light irradiation, resulting in faster decolouring kinetics. In connection with the self-cleaning performance, these same SPs preserved the photoinduced hydrophilicity of the lime mortars, reaching good wettability of the surface of the mortars (water contact angles of ca. 10º), even in the presence of the sodium oleate, proving the compatible characteristics of the admixtures and allowing obtaining a new range of actively depolluting lime mortars.

Keywords: lime mortar, photocatalyst, superplasticizer, depolluting, TiO_2, dispersion, NO removal, selectivity, self-cleaning

1. Introduction

Different strategies may be adopted to reduce the atmospheric pollutants (NO_x, SO_x, CO, H_2S, NH_3…) and to avoid the dirt accumulation and the subsequent deterioration of the construction materials (Luna et al., 2019; Pérez-Nicolás et al., 2018; Saeli et al., 2018; Xia et al., 2020; Krishnan et al., 2018; Pozo-Antonio and Dionísio, 2017), including the design of photocatalytic materials with depolluting and self-cleaning abilities (Krishnan et al., 2018; Luna et al., 2020; Munafò et al., 2015; Pérez-Nicolás et al., 2015).

The use of photocatalysts has been efficiently employed for the removal of gaseous contaminants with harmless end products (Folli et al., 2012; Lucas et al., 2013; Pérez-Nicolás et al., 2018; Dalton et al., 2002). Photocatalytic agents must be immobilized onto supporting materials, so that their incorporation in construction materials is one valuable option. The exposed areas of building materials facilitate the interaction between atmospheric pollutants and photocatalysts, reducing the concentration of pollutants in the surrounding environment (Luna et al., 2019) and degrading the dirt deposits, thus allowing the building material to display a self-cleaning behaviour. This self-cleaning effect is also observed in hydrophilic surfaces, in which the drops of water spread on the surface of the material, giving rise to a flowing aqueous film capable to sweep along dirt and dust (Son et al., 2012). Under illumination, photocatalysts exhibit photo-induced hydrophilicity, which, together with their photocatalytic activity, yield proved self-cleaning materials.

These building materials, incorporating photocatalysts, may become a good alternative for their use as new construction materials. In that way, the recourse to construction materials will reduce the air pollutants in the vicinity of the buildings and will circumvent the problems related to the dirt and dust accumulation, preserving the structure from damages, keeping the aesthetics of the edifications, particularly those of the Cultural Heritage, and leading to a reduction in maintenance and cleaning costs (Kapridaki et al., 2019, 2018; Luna et al., 2019; Pérez-Nicolás et al., 2018). Environmental factors should be considered for real applications, since they may affect the durability of the photocatalytic materials and their efficiency (wind speed and

direction, temperature, relative humidity, light irradiance, removal of photocatalytic particles…) (Guerrini et al, 2012.; Ballari and Brouwers, 2013; Diamanti et al. 2015; Guo et al. 2016; Lettieri et al. 2019; Carmona-Quiroga et al., 2018; Colangiuli et al. 2019).

Mortars, renders or grouts have been explored as materials able to accommodate photocatalysts added in bulk (Pérez-Nicolás et al., 2017; Ruot et al., 2009). The current work pursues the design of new lime mortars, which are attracting the interest of the scientific community as valuable repair materials (Azeiteiro et al., 2014; Salavessa et al., 2013). It has been reported that, in the architecture, the use of lime is currently gaining a renewed interest and internal plastering mortars, lime concrete or limecrete structures can be designed for modern building construction (Martínez-García et al, 2019). The use of lime mortar exhibits several potential advantages in terms of the sustainable development of these materials: their production has been reported to produce less environmental footprints, due to the lower energy consumption and CO_2 emissions as compared with cement (Giosuè et al., 2020). Some lime-based binders have been found to be carbon-negative building materials, such as hemp-lime concrete (Arehart et al., 2020; Arrigoni et al., 2017; Walker and Pavía, 2014) and, the use of pozzolans as binder substitutes lowers the initial emissions associated to the binder production (Arehart et al., 2020). The local availability, low processing level, capacity of recovering traditional methods of construction and the healthy nature of the compound can be also mentioned as advantageous aspects of the use of lime (Arrigoni et al., 2017; Deng et al., 2020; Orsini and Marrone, 2019).

Furthermore, the use of lime may be effective in reducing the NO_2 release, which has been pointed out as one of the drawbacks of the photocatalytic NO abatement (Bloh et al., 2014). NO_2 toxicity is higher than that of the NO and may act as precursor of other harmful components (Yang et al., 2018). The proved high NO_2 adsorption of the portlandite confirms the lime binders as suitable hosting matrices for photocatalysts, with ability to increase the selectivity of the NO removal (Kaja et al., 2019; Krou et al., 2013; Zhang et al., 2008).

These mortars could be applied as one-coat rendering mortars, as multilayer renders or as repointing materials, both in modern buildings and in repair works of the Cultural Heritage (Giosuè et al., 2018). These new finishing mortars, which offer large exposed

areas favourable for depolluting purposes, should at the same time be durable and show self-cleaning ability. To this aim, the novelty of this work includes the obtaining of air lime mortars with simultaneous combination of different admixtures added in bulk including: (i) a mineral admixture (pozzolanic nanosilica), which imparts strength and durability (Nunes et al., 2016; Sharma et al., 2019; Tsardaka and Stefanidou, 2020); (ii) a waterproofing agent (sodium oleate) to reduce the water absorption and the detrimental effects of the water movements (Falchi et al., 2015; Silva et al., 2020); (iii) nano-TiO_2, as the most popular metallic oxide semiconductor photocatalyst (Crupi et al., 2018; Folli et al., 2012; Haider et al., 2019; Zouzelka and Rathousky, 2017); and (iv) a superplasticizer (up to five different ones were assayed: four based on polycarboxylated-ether derivatives and one poly-naphthalene sulfonate (Padovnik et al., 2016; Padovnik and Bokan-Bosiljkov, 2020; Puertas et al., 2005; Silva et al., 2019)). The compatibility between all these types of admixtures in lime mortars is still pending of investigation and some of the admixtures might ruin the expected action of others. For example, the use of a waterproofing agent might reduce the necessary water access to the active sites of the photocatalyst, thus reducing its efficiency. In photocatalytic coatings, the compatibility between TiO_2 and hydrophobic compounds has been tackled and found to be dependent on the optimal ratios between these two components (La Russa et al., 2016; Scalarone et al 2012; Cappelletti et al., 2015; Manoudis et al., 2009; Calia et al. 2015). After the obtaining of the new self-cleaning and depolluting air lime mortars, this work investigates the two main following issues.

On the one hand, the effect of the superplasticizers on the photocatalytic effect of the mortars was studied. These dispersing admixtures were added with the purpose of overcoming one of the problems related to the use of photocatalysts, which is the charge carriers recombination that results in a low quantum efficiency and, accordingly, a low depolluting effectiveness (Araña et al., 2019; Mamaghani et al., 2017; Wang et al., 2020; Zouzelka and Rathousky, 2017). The electron-positive hole coupling due to the proximity between active sites is a major drawback, jeopardizing the efficiency of the photocatalytic action. This vicinity may be a direct consequence of the choice of nano-sized compounds, which, while being positive because they offer more surface area and thus active sites, show at the same time a sharp trend to agglomerate reducing the catalyst area (Yang et al., 2019). The calcium-rich and highly alkaline environment in lime or cement mortars has been reported as an additional factor explaining the

efficiency drop, since the precipitation of $Ca(OH)_2$ and $CaCO_3$ may cover TiO_2 active sites (Yang et al., 2019). The use of suitable superplasticizers can lead to an effective separation of the TiO_2 nanoparticles increasing the photocatalytic activity. Compatible superplasticizers with air lime, which had been proved to be effective when applied as coatings (Pérez-Nicolás et al., 2018), were thus tested in these new mortars in bulk addition. The depolluting activity of the mortars was assessed by monitoring the NO_x degradation in a closed reactor. The release of intermediate toxic NO_2 was also assessed and the selectivity values of the new mortars were calculated. The self-cleaning ability was determined by dye-degradation measurements.

On the other hand, the influence of the admixtures, particularly the waterproofing one, on the photo-induced hydrophilicity was also investigated. Whilst, according to the literature, the addition of a water repellent could be positive for increasing the frost resistance of the mortars (Falchi et al., 2013; Nunes and Slížková, 2016; Silva et al., 2020, Izaguirre et al., 2009 and 2010) by reducing the water uptake (Silva et al., 2020; González-Sánchez et al, 2021), its presence might interfere with the hydrophilicity, thus endangering the self-cleaning performance. The compatibility between the presence of the waterproofing admixture and the self-cleaning effect was therefore studied.

2. Materials and methods

2.1 Materials and composition of mixtures

For the preparation of the mortars, hydrated calcitic lime CL-90 was used as a powder, supplied by CALINSA, Navarra, Spain. This lime has a composition of 68.5% CaO, 3.3% MgO, 1.4% SO_3 and 1.0% SiO_2. The particle size of the powdered lime was 10 µm (less than 10% > 50 µm). A fine limestone aggregate supplied by CTH (Huarte, Navarra, Spain) with a particle size less than 2 mm was also used. The granulometry of the aggregate has been published elsewhere (González-Sánchez et al., 2020). The preparation of the mortars was made using a 1 to 3 weight ratio of binder/aggregate (González-Sánchez et al., 2020; Izaguirre et al., 2011). In order to separate and to identify the effect of the admixtures, the mixing water was fixed at a 28%, which was the percentage able to yield a settlement diameter of 165 mm in the control sample, as measured in the flow table test according to EN 1015-3 (European Committee for Standardization, 2006). Slump values of each sample are provided in the Supplementary material (Table S1)

The following admixtures were also added to prepare the mortars. Detailed composition of each one of the samples is displayed in Table 1. The percentages of admixtures are expressed by weight of lime (bwol):

- Pozzolanic mineral admixture (20%): Nanosilica (NS), provided by ULMEN Europa S.L. as a colloidal superplasticizer-free silica suspension. Fig. 1 shows the TEM analysis of this admixture, with average particle size of ca. 50 nm and a specific surface area of ca. $500\ m^2\ g^{-1}$ (established by BET nitrogen adsorption isotherms) (Fernández et al., 2013; Navarro-Blasco et al., 2014).
- Waterproofing agent (0.5%): Sodium oleate (O) (HISA A 2388 N). Its molecular weight is of 304 g mol^{-1}. The structure and performance of this admixture has been described by Izaguirre et al. (Izaguirre et al., 2009).
- Photocatalytic agent (T) (2.5%): Nanoparticles of bare titanium dioxide (TiO_2) as photocatalyst supplied by Aeroxide P25, Evonik. The particle size of the photocatalyst, 21 nm, was ascertained in previous research by Pérez-Nicolás et al. (Pérez-Nicolás et al., 2017). Fig. 1 shows the TEM micrograph of this admixture, evidencing its tendency to agglomerate.
- Superplasticizer (SP) (added in two different dosages 0.5% and 1%): the following superplasticizers were tested: four different polycarboxylate-based polymers and a polynaphthalene sulfonate PNS were used. A complete characterization of their structures was reported in previous works (González-Sánchez et al., 2020; Pérez-Nicolás et al., 2018). Most relevant characteristics are summarised below:
    - PCE-A, molar mass 8.00×10^3 and specific anionic charge 920 μeq/g
    - PCE-B, molar mass 4.60×10^4 and specific anionic charge 1695 μeq/g
    - PCE-C, molar mass 3.84×10^4 and specific anionic charge 2740 μeq/g
    - PCE-D, molar mass 3.16×10^4 and specific anionic charge 1895 μeq/g
    - PNS, molar mass 1.40×10^5 and specific anionic charge 4089 μeq/g

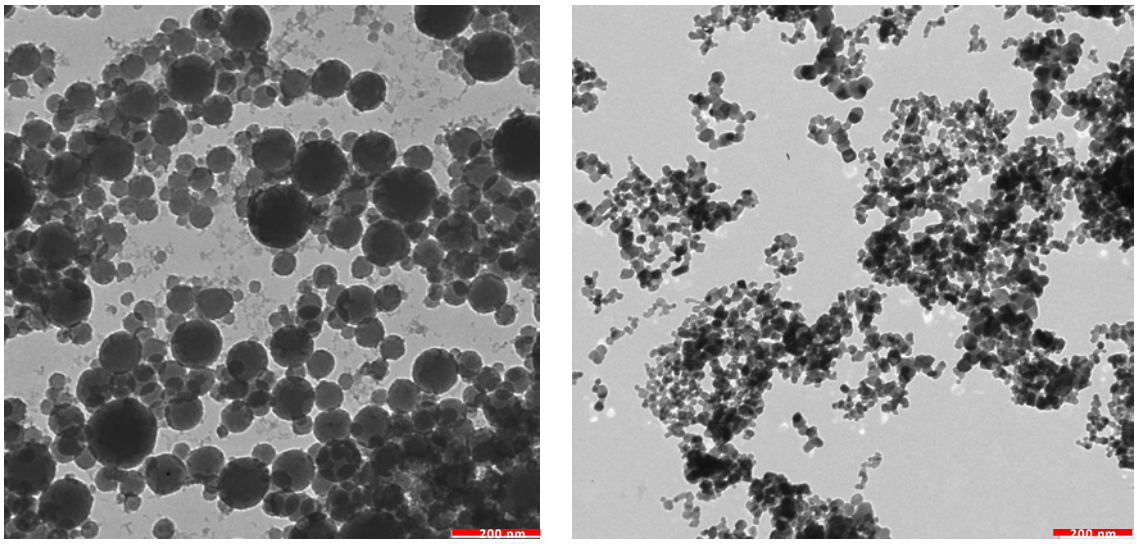

Fig. 1. TEM micrographs of nanosilica (left) and nano-TiO_2 (right)

Table 1. Assayed samples: percentage composition of the admixtures

	Name	Nanosilica (NS)	Sodium oleate (O)	TiO_2 (T)	Superplasticizer
Control	**L**	-	-	-	-
Superplasticizer-free samples	**O-T**	-	0.5	2.5	-
	NS-T	20	-	2.5	-
	O-NS-T	20	0.5	2.5	-
PCE-A	**A0.5**	-	0.5	2.5	0.5
	A1	-	0.5	2.5	1.0
	A0.5-NS	20	0.5	2.5	0.5
	A1-NS	20	0.5	2.5	1.0
PCE-B	**B0.5**	-	0.5	2.5	0.5
	B1	-	0.5	2.5	1.0
	B0.5-NS	20	0.5	2.5	0.5
	B1-NS	20	0.5	2.5	1.0
PCE-C	**C0.5**	-	0.5	2.5	0.5
	C1	-	0.5	2.5	1.0
	C0.5-NS	20	0.5	2.5	0.5
	C1-NS	20	0.5	2.5	1.0
PCE-D	**D0.5**	-	0.5	2.5	0.5
	D1	-	0.5	2.5	1.0
	D0.5-NS	20	0.5	2.5	0.5
	D1-NS	20	0.5	2.5	1.0
PNS	**P0.5**	-	0.5	2.5	0.5
	P1	-	0.5	2.5	1.0
	P0.5-NS	20	0.5	2.5	0.5
	P1-NS	20	0.5	2.5	1.0

2.2. Preparation of mixtures

All raw materials (lime, aggregates and admixtures) in the planned proportions were mixed for 5 minutes in a solid-admixtures mixer BL-8-CA (Lleal, S.A.). Afterwards, the resulting mixture was poured into a different Proeti ETI 26.0072 mixer (Proeti) and water was added and mixed for 90 s at low speed and adjusted according to EN 196-1 (European Committee for Standardization, 2005).

Cylindrical moulds (36 mm height and 40 mm diameter) were used to prepare the hardened specimens. Samples were demoulded after 7 days and stored at the same curing conditions (20 °C and 60% RH). Curing ages were 28 and 91 days. Properties were then investigated. At least three replicates of the mortars were tested per curing age and per studied property to obtain representative results. For some analyses, a Struers cutting-polishing machine was used to obtain slices (10 mm height and 40 mm diameter) from the cylindrical specimens.

2.3 Methods

2.3.1 Photocatalytic activity: NO_x abatement

A continuous flow experiment adapted from an ISO standard method was used for this assay (Draft International Standard, 2007). The experimental system includes a cylindrical photoreactor (height 12 cm; diameter 14 cm), fed by a 0.78 L min^{-1} flow of nitrogen and air with an initial concentration of 500 ppb NO and around 20 ppb of NO_2 (in all instances accurately and continuously monitored by means of a Environnement AC32M chemiluminescence detector). The conditions established were 50 ± 5% RH and 25 ± 2 °C; a Osram Ultra Vitalux 300W lamp was used to supply UV-vis illumination (Corrêa, 2015). The nominal irradiance of the lamp after 1 h and at a 0.5 m of distance was of 41.4 W m^{-2} (780-380 nm), 13.6 W m^{-2} (400-315 nm) and 3.0 W m^{-2} (315-280 nm). This lamp combines visible, UVA and UVB radiation achieving a good simulation of the solar light (Heikkilä et al., 2009; Prieto and Lagaron, 2020). Experiments were carried out for each sample discs of 91 days-cured mortars, with 25.14 cm^2 of total exposed area. While the sample was inside of the reactor and the lamp off, the NO_x stream was flowed 10 minutes to stabilize the NO concentration in the reactor, allowing reaching the adsorption equilibrium between the NO_x and the

sample. Afterwards, lamp was switched on for 30 minutes. Then, the lamp was turned off for 10 min, allowing the recovering of the initial NO concentration value. The selectivity values were calculated as the percentage ratio NO_x/NO, high values meaning a very limited NO_2 release and thus a more effective total NO_x degradation. The error analysis of the experimental, expressed in terms of relative standard deviation, was calculated under reproducibility conditions at 3.3% from the repeated analysis of at least three identical samples.

2.3.2 Determination of density, air content, workable life, pore size distribution and compressive strength of the mortars

In the fresh mixtures, the density, air content and workable life (expressed as the time needed to reach stiffness in the mortar) were determined according to the standards EN 1015-6, 1015-7 and 1015-9 (European Committee for Standardization, 1999a, 1999b, 1999c). Values are collected in the Supplementary material (Table S1).

Mercury intrusion porosimetry (MIP) measurements (Micromeritics-AutoPoreIV-9500) were used to establish the pore size distributions of the hardened mortars after both curing ages. The samples were analyzed at a pressure range of 0.0015–207 MPa.

A Proeti ETI 26.0052 compression machine (Proeti) was utilized to measure compressive strengths after 28 and 91 curing days of the cylindrical mortars. The assays were executed at a breaking speed 5–50 KP s^{-1} and a time interval between 30 and 90 s,

2.3.3 Adsorption of the superplasticizers and zeta potential studies

In order to know the adsorption of superplasticizers on TiO_2, a batch adsorption experiment was carried out. Five reference samples with 10 mg of each SP and 5 suspensions with the same amount of SP plus 500 mg of TiO_2 were prepared and made up to a final volume of 50 mL. Samples were mechanically stirred for 30 min to reach the adsorption equilibrium and were subsequently centrifuged for 2 hours at 8000 rpm in a Heraeus Biofuge Stratos wobbler. Then the supernatant was taken, and the total organic carbon (TOC) was determined in a TOC-L Shimadzu total organic carbon analyzer. The adsorbed amount of superplasticizer was thus calculated as the difference between the TOC content of the reference samples and the TOC content of the supernatant of the suspensions.

The surface charge of the different suspensions was monitored with a Zeta potential electroacoustic analyzer (ZetaProbe Analyzer, Colloidal Dynamics). First, two different initial media were prepared: one, a suspension in water of nano-TiO_2 particles; other, a mixture of air lime, water, NS and sodium oleate, using the same relative compositions described in Table 1. The media were stirred for 30 minutes. Then, different polymer-based superplasticizers solutions (1% w/v) were used as titrant media solutions, and zeta potential values were continuously monitored.

2.3.4 TG studies

The rate of carbonation of hardened samples was analyzed at 28 and 91 curing days using alumina crucibles by thermogravimetric studies in a simultaneous TG-sDTA 851 Mettler Toledo thermoanalyzer device at 10 °C min^{-1} heating rate, under static air atmosphere were heated from 25 until 1000 °C. A slice of the cylindrical specimens (10 mm height and 40 mm diameter) was powdered and homogenized in an agate mortar and ca. 0.050 g were thus taken to be analyzed. The percentages of weight losses around 450-480 ºC were ascribed to the dehydroxylation of the uncarbonated portlandite, whereas the weight losses at ca. 800-900 ºC were attributed to the CO_2 release from the calcium carbonate.

2.3.5 Self-cleaning test

The self-cleaning capacity of all samples was evaluated by studying the dye degradation in mortars exposed to UV-Vis light. First, the surface of the discs was stained with three layers of an aqueous solution of organic dye rhodamine B (1 mM) applied by brushing. Samples were left to dry in an oven at 50ºC for 60 min. Subsequently, the discs were irradiated under the Osram Ultra Vitalux UV-Vis lamp of 300 W (data of irradiance above mentioned in section 2.3.1). The photodegradation activity (discoloration of the surface of the mortars) was evaluated at 5 time intervals (5, 20, 80, 140 and 310 min) using a Konica-Minolta CM-2300d colorimeter. Measurements were carried out in 9 circular regions (diameter 3 mm) for each stained sample surface and the color variations over time were obtained by the chromatic coordinates a^* and b^*. With the data obtained, the normalized color change (ΔC_n) as Chroma variation was calculated with follow equation (Fornasini et al., 2019):

$$\Delta C_n = \sqrt{\frac{\left[a_t^* - a_0^*\right]^2 + \left[b_t^* - b_t^*\right]^2}{\left[a_C^* - a_0^*\right]^2 + \left[b_C^* - b_t^*\right]^2}} \qquad \textbf{Eq. 1}$$

where a_t^* and b_t^* are the coordinates at irradiation time t, whereas a_C^* and b_C^* are measured on the clean stones before staining with dye. The value 1 would correspond to the complete dye degradation. Finally, results were reported as a function of the irradiation time.

2.3.6 Surface wettability and photo-induced hydrophilicity

The evaluation of the surface wettability and the photo-induced hydrophilicity of the different samples was performed by OCA 15EC (DataPhysics Instruments GmbH) equipment measuring the static water contact angle (CA) of the samples under illumination with an Osram Ultra Vitalux 300 W lamp at 0, 1, 3, 5, 8 and 30 min. Onto the surface of the hardened grouts, five water droplets of 5 μL were put at five different points, and the results were expressed as averages of these measurements.

3. Results and discussion

3.1 NO_X removal: effect of the porosity and role of the superplasticizers

The values of the fresh state properties of the mortars reported in Table S1 show that the SPs increased the fluidity of the mortars but also the workable life (Duran et al, 2018; Fernández et al., 2013; González-Sánchez et al., 2020). Due to the dual nature of some of the admixtures, oleate for example, they partially acted as surfactants, and thus the entrained air also increased (Izaguirre et al., 2009; Silva et al., 2020). It must be emphasized that these mortars do not present optimized ratios of the components, since, as explained in section 2.1, the water/lime ratio was kept constant (28% with respect to the weight of lime plus aggregate) to assess the effect of the admixtures.

The photocatalytic activity was assessed by monitoring the nitrogen oxide removal ability of the mortars after 91 curing days in a closed reactor and the percentages of the NO and NO_x removal are depicted in Fig. 2. The patterns of the NO abatement tests followed the general trend reported in previous works (Ângelo et al., 2013; Pérez-Nicolás et al., 2018, 2017) and showed in Fig. S1 (Supplementary material): in dark conditions, NO values were left to stabilize in order to drive out the adsorption

phenomenon. When the light was switch on, a quick decrease of the NO concentration was observed. Samples reached a plateau, which also showed a slight trend to decrease along the time of exposure, unlike some other results that showed a tendency to increase (Jin et al., 2019). This finding can be ascribed to an unsaturation state, suggesting the presence of free active sites able to degrade more NO molecules.

As it can be seen in Fig. 2, the addition of nano-TiO_2 dramatically increased the NO abatement, in comparison with the control sample (L, TiO_2-free). The removal of up to 6% of NO in the control sample is ascribed to the photolysis of the pollutant and to the sorption and conversion of NO into nitrous acid (not measured) (Gandolfo et al., 2015; Zouzelka and Rathousky, 2017). The addition of the nano-structured photocatalytic admixture increased the NO removal up to a 28-37% range (for samples O-T, NS-T and O-NS-T). In comparison with these samples, the use of dispersing admixtures sharply increased by 33% the NO abatement (the percentage of NO removal of mortars with superplasticizers was 44% on average). These results are a clear evidence of the usefulness of incorporating superplasticizers in lime mortars to achieve a suitable dispersion of the TiO_2 within the binding matrix, which had been highlighted as one of the challenging issues in cementitious binders (Yang et al., 2019).

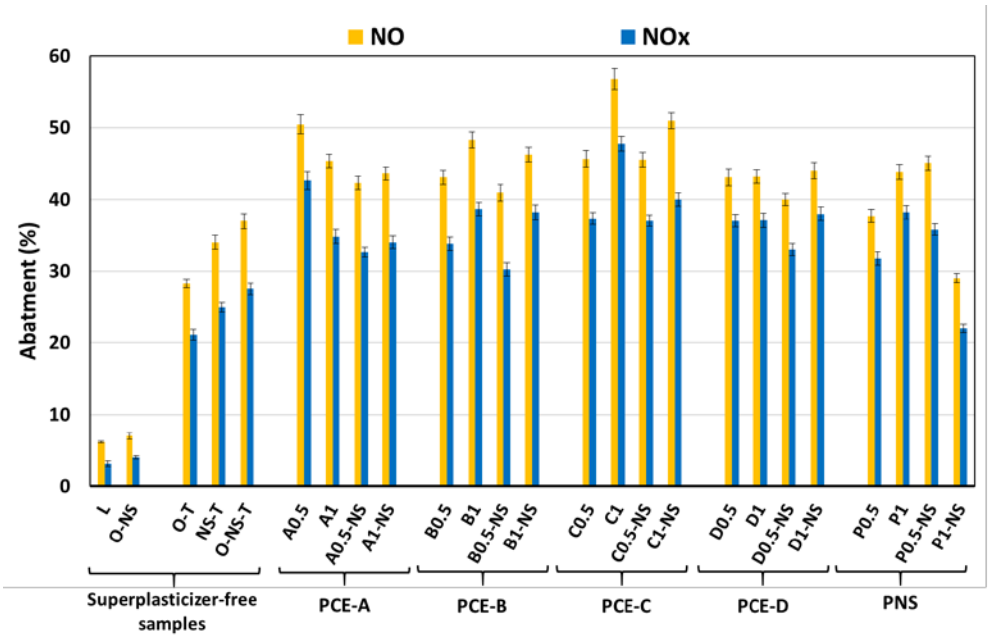

Fig. 2. NO and NO_x abatements for different samples under UV-Vis irradiation.

3.1.1 Influence of the porosity

The effect of the pozzolanic admixture addition was found to be dependent on the composition of the mortar. For superplasticizer-free mortars, the addition of NS

enhanced the NO removal. The refinement of the pore structure accounts for this finding: for samples with NS (NS-T and O-NS-T), the population of capillary pores between 0.01 and 0.1 µm increased, as it was observed in the pore size distribution graphs of mortars (91 curing days), depicted in Fig. 3. These pores act as a booster of the photocatalytic activity, as stated by Kaja et al. (Kaja et al., 2019) in cement mortars with TiO_2. These authors concluded that the formation of capillary pores in the range 0.01-0.05 µm was critical for the enhancement of the photocatalytic activity (NO abatement). In the current work, sample O-T without NS showed negligible porosity in that pore range, yielding a 28% of NO removal. The samples with NS (NS-T and O-NS-T), with an outstanding increase of capillary pores in that pore range, increased the NO degradation 1.2-1.3 times.

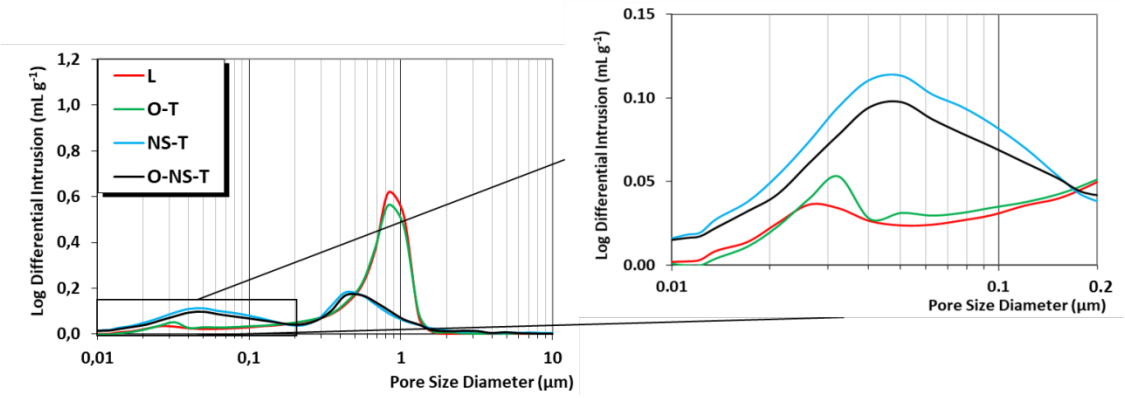

Fig. 3. Pore size distribution of superplasticizer free samples (91 curing days)

However, in samples with SPs, the addition of nanosilica depicted a different performance. As a general tendency, samples with NS showed a lower abatement of NO. The porous structure contributes to clarify the reasons for this lesser performance. The addition of SPs modified the pore size distribution of the samples with NS, nano-TiO_2 and lime. Instead of increasing the capillary pores between 0.01 and 0.1 µm (as reported for air lime mortars with additions of NS (Duran et al., 2014)), the presence of the superplasticizers caused a clear decrease of the population of the pores of this range (Fig.4). This fact had been also observed in previous works dealing with NS and SPs (Fernández et al., 2013; Pérez-Nicolás et al., 2016) and was related to the inhibition of the pozzolanic reaction (Pérez-Nicolás et al., 2016) and to the enhancement of the filling effect of the better dispersed NS within the network of lime particles (Alvarez et al., 2013).

Due to the use of the same ratio of mixing water (see section 2.1), the presence of a high-range water-reducer, a superplasticizer, produced a large excess of water which in the end evaporated causing the main contribution to the pore size distribution (main pore peak at around 1-2 μm, which is larger than the most commonly reported 0.5 to 0.8 μm for air lime mortars (Duran et al., 2018; González-Sánchez et al., 2020; Lanas and Alvarez, 2003; Martínez-García et al., 2019; Santos et al., 2018). This shift of the critical pore diameter towards higher diameters and the increase observed in the area under the curve (meaning higher total porosity) influenced the values of the compressive strengths, which showed an expected drop with respect to the control (Fig. 5). Compressive values of the mortars were relatively low, in good agreement with reported values for air lime mortars (Lanas and Alvarez, 2003; Magalhães and Veiga, 2009). The final fate of these mortars, after the necessary dosage adjustments (particularly of water/lime ratio), would be their use in wide exposed areas (i.e. as one-coat or multi-layer rendering mortars). In these cases, the compressive strength values fulfil the general requirements reported by Veiga et al. (2010) for rendering mortars for the Built Heritage (compressive strengths ranging from 0.40 to 2.50 MPa). Actually, rendering mortars do not require large compressive strength values, since they do not perform as load bearing mortars. Even for cement-based rendering mortars, the standard EN 998-1 (European Committee for Standardization, 2016) prescribes compressive strength values of 0.4 MPa for type I, 1.5 MPa for type II and 3.5 MPa for type III as lower limits. All samples fulfil at least the requirements for type I and most of them for type II.

Samples with pozzolanic agent, NS, exhibited higher strength values as a consequence of the C-S-H formation and to the pore refinement discussed before. The samples with the most effective superplasticizers in terms of fluidity (slump values) (samples with PCE-B and PCE-C) yielded the lower values of compressive strength, due to the more marked influence of the excess of mixing water in comparison with the other superplasticizers. For practical applications of these samples, the water/lime ratio adjustment is imperative, especially for the NS-free ones exhibiting the lowest values (see Fig. 5).

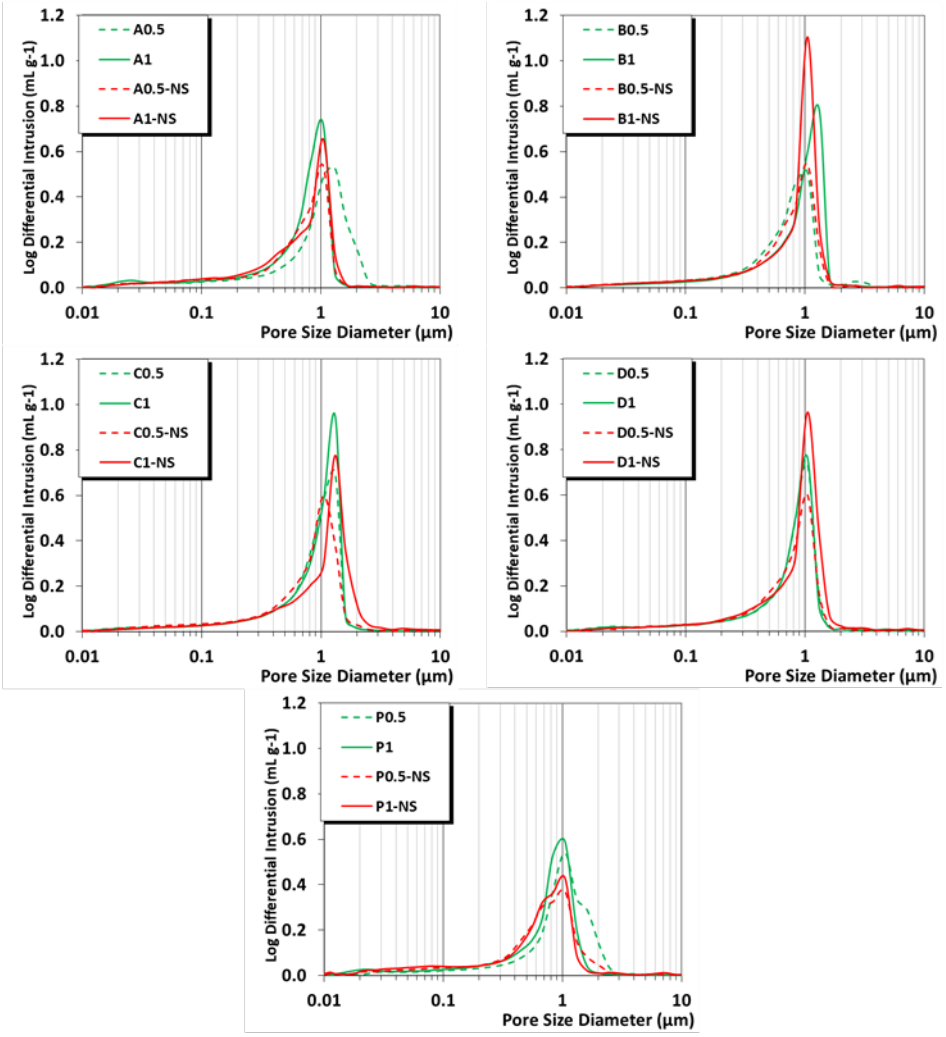

Fig. 4. Pore size distribution of samples with different superplasticizers (91 curing days)

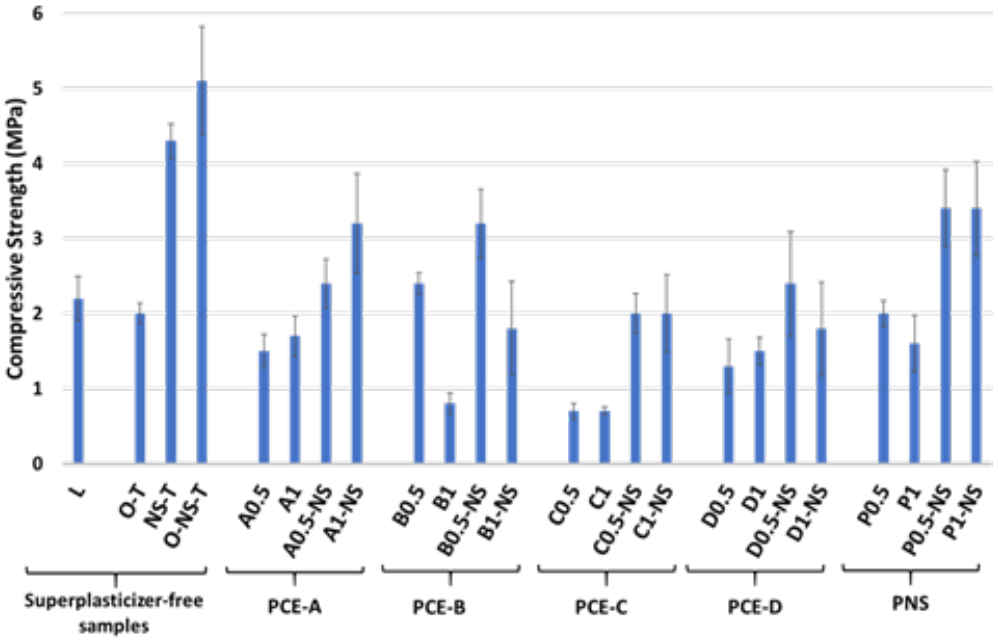

Fig. 5. Compressive strength of the different samples after 91 curing days

Despite the absence of the capillary pores from 0.01 to 0.1 μm, the NO abatement of these mortars was higher than that of the SP-free mortars (Fig. 2). This finding can be tentatively ascribed to the combination of the following factors: (i) the macroporosity increase, in line with the work by Sugrañez et al. (Sugrañez et al., 2013). These authors reported a better photoactivity and thus a higher NO degradation in cement mortars with a greater amount of macropores > 2 μm. (ii) The achievement of an efficient TiO_2 dispersion because of the presence of superplasticizing admixture.

Concerning the first factor and ruling out the influence of the pores between 0.01-0.1 μm for samples with SP, the effect of the total porosity was considered. Fig. 6 shows the influence of the total porosity on the NO abatement (photocatalytic activity) for SP-free samples and for mortars with each one of the tested SPs. The results showed that there is not a clear correlation between these parameters. A high porosity of the mortar (> 38%) does not necessarily involve a high NO removal rate. This can be noticed, for example, for P1-NS, P0.5 and samples with PCE-D, which despite their high total porosity exhibited NO removal percentages around 40% or lower. The opposite is also true. Mortars with comparatively lower total porosity (32-36%) yielded high NO abatements (> 45%). The small slopes of the correlations confirm the absence of any significant influence of the total porosity. This is in line with previous works in the literature that state that a high porosity does not necessarily involve a high photoactivity (Strini, Cassese, Schiavi, 2005; Jiménez-Relinque et al., 2015).

The influence of the pore size distribution (PSD) has been reported in previous works about cement-based mortars with TiO_2, and some contradictory results have been obtained: whereas Jiménez-Relinque et al. (2015) found that the most important pore sizes fostering the NO abatement were found to be between 0.5 and 0.05 microns, whereas Haka et al. (2019) concluded that pores between 0.01 and 0.05 microns are the critical ones for the NO degradation. In addition, other factors are also relevant, such as the surface roughness (or, more accurately, the available surface active) (Jiménez-Relinque et al., 2015).

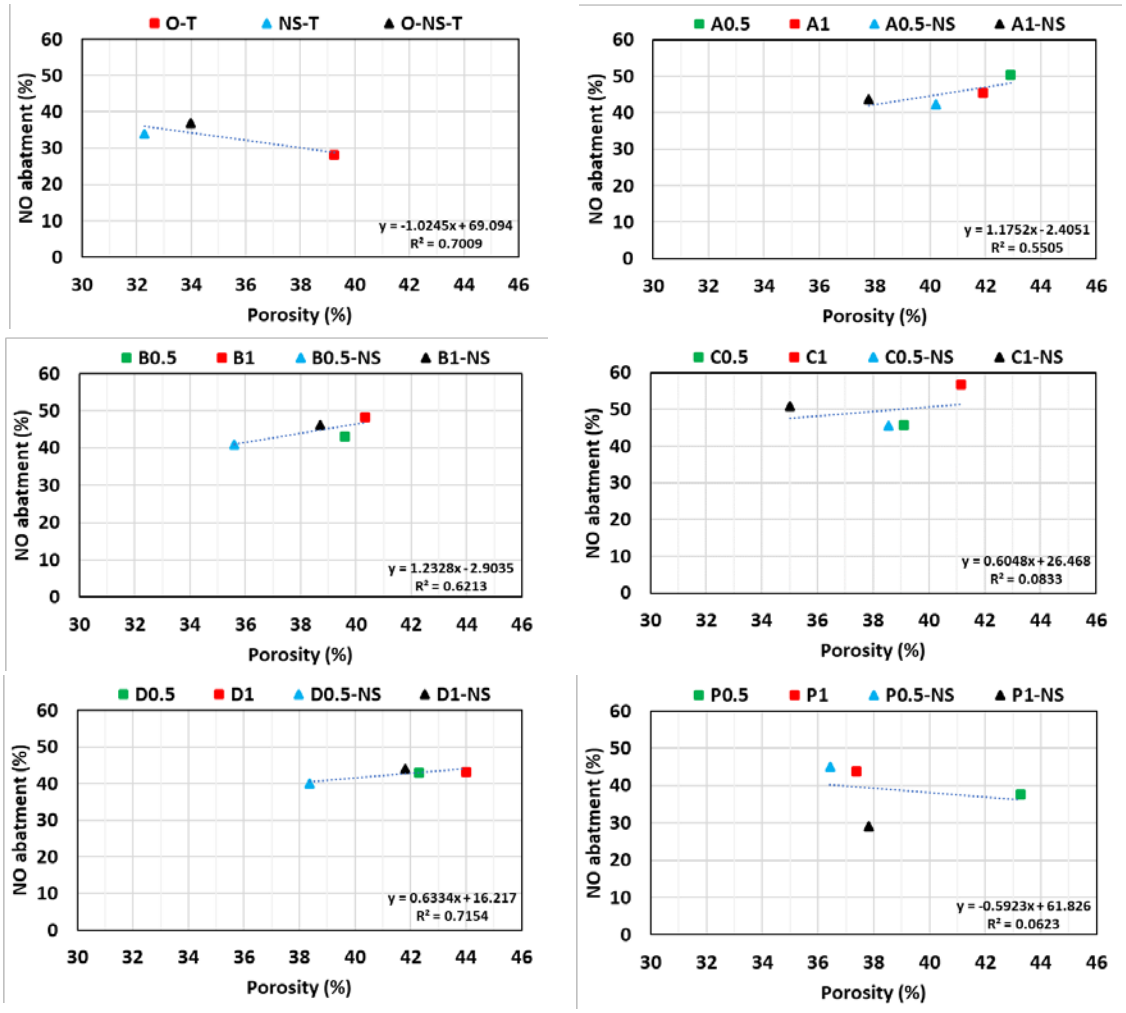

Fig. 6. Influence of the total porosity (%) on the NO abatement (%).

As explained before, the absence in the tested lime mortars of the capillary pores from 0.01 to 0.1 μm does not allow to argue them as the explanation of the NO degradation. Lime mortars depict a very different PSD than that of the cement-based mortars. The influence of the macroporosity (pores ≥ 1 μm) on the NO abatement was also studied. The graph is presented in Fig. 7 and a significant correlation ($p < 0.01$) was identified altogether, confirming the influence of the macropores ≥ 1 μm in the photoactivity of mortars with TiO_2 (Sugrañez et al., 2013). As an explanation to this importance of the pores in this range, it must be considered that the pore size distribution of these lime mortars fits a unimodal and really simple distribution, as it can be seen in Fig. 4. All samples exhibit PSD, in which the macropores around 1 μm act as critical pore diameter, i.e, the maximum pore diameter that connect the larger pores. This diameter indicates the connectivity of the pores: the formed network of pores is related to the gas permeability, and therefore is related to the photocatalytic abatement of the NO in these lime mortars. Actually, in these lime mortars, the macropores ≥ 1 μm would be the

responsible to allow the pollutants and also the light to access into the internal structure of the mortar.

However, it is evident that the changes in the region of the critical pore diameter and in the macropores within the mortars with SPs are not enough by themselves to explain the photocatalytic activity. There are some acute NO abatement differences among samples with similar macroporosity ≥ 1 μm, as for example samples P1-NS and B0.5 (with 29 and 43%, respectively, of NO abatement) or samples B1-NS and C1 (46 and 57% of NO abatement). Therefore, the second factor, i.e. the effectiveness of the dispersion of TiO_2 by the SPs, should be then taken into account to understand the photocatalytic activity of the tested mortars. Their different performance can be explained considering the molecular architecture of the superplasticizers and their action mechanism.

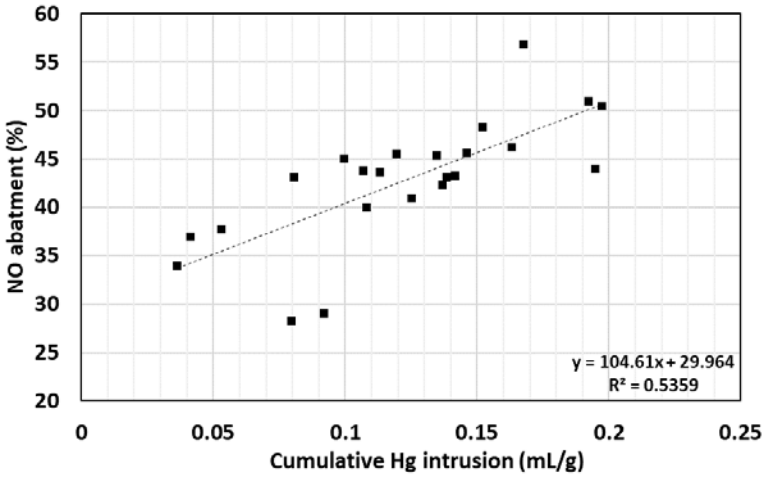

Fig. 7. Influence of the macroporosity (pores ≥ 1 μm, expressed as volume of intruded mercury per g of mortar) on the NO abatement (%).

3.1.2 Role of the superplasticizers

The NO degradation values (Fig. 2) showed that the lime mortars with polycarboxylate-based SPs yielded better NO removal percentages than those with PNS. Mortars with PCEs resulted in average NO removal values from 43% to 50%, while the average percentage for PNS was 39%. Among the tested PCEs, PCE-C degraded on average 50% of NO resulting in the highest rates of NO removal. PCE-A and PCE-B exhibited the same NO abatement percentages (average values of 45%), while the percentage for PCE-D was slightly lower (43%).

The different polymeric structures of the superplasticizers have a clear influence on their dispersing ability. In previous studies it has been pointed out that the

polynaphthalene sulfonate has a linear structure, with a high number of anionic groups (sulfonates), which allow the PNS to be strongly adsorbed onto the different particles (Crépy et al., 2014; Duran et al., 2018; González-Sánchez et al., 2020; Mezhov et al., 2020). In Fig. 8 the zeta potential titration of aqueous nano-TiO_2 dispersion with PNS depicts the charge reversal phenomenon caused by the intense PNS adsorption (experimentally determined to be 77% onto these particles) and its high anionic charge density.

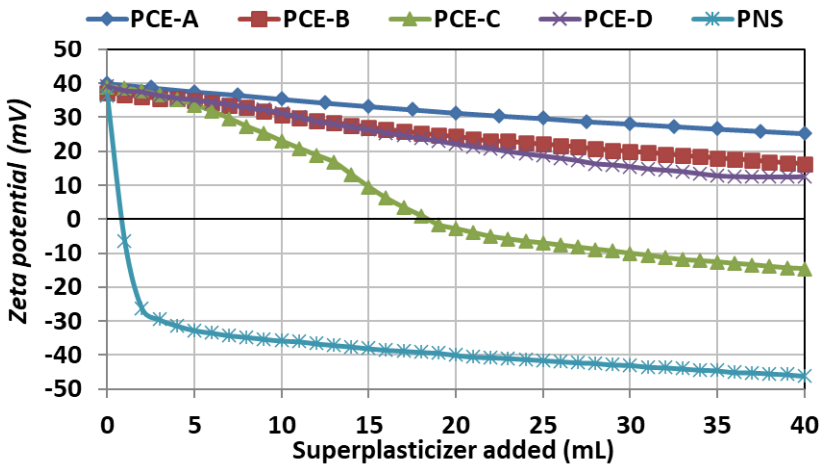

Fig. 8. Zeta potential titration of aqueous nano-TiO_2 dispersion with different superplasticizers

On the other hand, PCE-based admixtures have been described as branched polymers, with a main central backbone with ionizable carboxylate groups and side chains with variable length (Fediuk et al., 2019; Puertas et al., 2005; Zhang and Kong, 2015). As reported in section 2.1, the anionic charge densities of these PCEs are lower than that of the PNS, explaining why their zeta potential curves are quite different. In Fig. 8, the charge reversal only took place for PCE-C, which has more carboxylate groups than the other PCEs and shows more adsorption onto TiO_2 particles (76%) than, for example PCE-B and PCE-D (adsorption values of 68% and 52%, respectively). However, the IEP (isoelectric point) for PCE-C was achieved after the addition of higher amounts of SP in comparison with the PNS. The addition of PCE-A hardly changed zeta potential because, despite its 79% of adsorption, its low number of carboxylate groups did not substantially modify the charge at the surface of the TiO_2 particles.

It is generally assumed that at pH of the assay the adsorption is mainly driven by hydrogen bonds between the SPs and the $TiOH/TiOH_2^+$ groups at the surface of the

TiO_2 particles, influenced also by the molecular weight of the polymers (Liao et al., 2009; Liufu et al., 2005).

However, the effectiveness in the dispersion of the nano-TiO_2 particles in the complex medium of the fresh lime mortar does not depend mainly on an electrostatic repulsion action. Whilst the PNS shows a working mechanism based on electrostatic repulsions (Mezhov et al., 2020), the PCEs have been proved to combine electrostatic repulsions with steric hindrance (Baltazar et al., 2013; Crépy et al., 2014; Puertas et al., 2005; Silva et al., 2019). In the literature, this electro-steric working mechanism was confirmed by far as more efficient in lime systems than the mere electrostatic one (González-Sánchez et al., 2020; Yoshioka et al., 1997). Other factors that must be considered are the anchorage of the SPs onto the particles, necessary for an effective dispersion (Plank and Yu, 2010; Seabra et al., 2007), and the length of the side chains of the PCEs, responsible for the steric-based dispersion (Plank and Yu, 2010; Yoshioka et al., 1997).

Fig. 9 shows the zeta potential curves of titration of the simulated complex systems of the mortars (lime, nano-TiO_2, sodium oleate and NS) with the SPs. In order to interpret these curves, it must be considered that, at the highly alkaline pH of the lime medium, the following groups at the surface of the different particles should be ionized and thus negatively charged: portlandite particles, C-S-H phases (formed because of the pozzolanic reaction between lime and NS) and the nano-TiO_2 particles. These negatives surfaces were expected to be strongly sheltered by a layer of positive calcium counter-ions, potential determining ions, explaining the positive zeta potential values at the beginning of the experiment and promoting the adsorption of negatively charged polymers (González-Sánchez et al., 2020; Pérez-Nicolás et al., 2018; Plank and Winter, 2008; Zhang and Kong, 2015). As it can be observed in Fig. 8, the gradual addition of PNS led to the systems to reach the IEP (zeta potential 0 mV). This finding implies that the dispersing action of PNS was inhibited, because this admixture has an electrostatic working mechanism (Mezhov et al., 2020).

Among the PCEs, Fig. 9 shows, in agreement with the higher NO abatement observed in mortars with this SP, how the titration with PCE-C allowed obtaining faster the positive zeta potential responsible for the electrostatic stabilization of the particles, which, together with the steric hindrance, is responsible for the effective dispersion in the assayed media. Similarly, the poorest photocatalytic performance in mortars with

PCEs was observed for PCE-D, which in Fig. 9 was seen to present a severe delay (high amount of SP required) in the achievement of the stabilization of the particles.

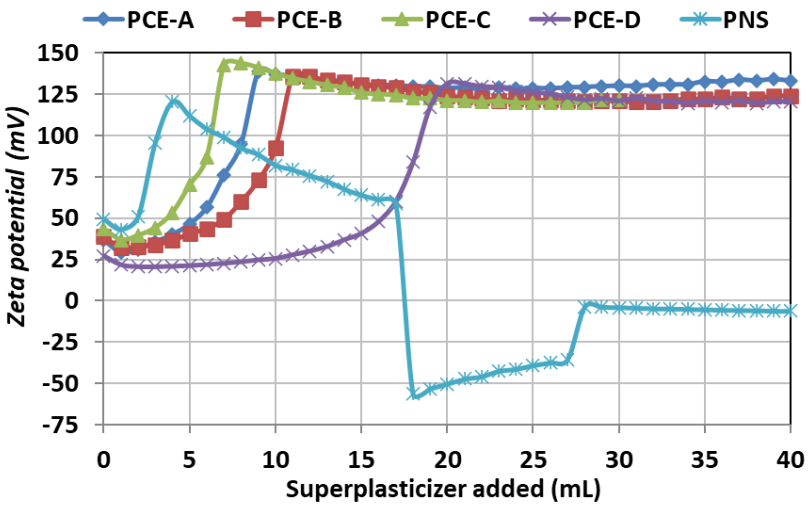

Fig. 9. Zeta potential curves of titration of the simulated complex systems of the mortars (lime, nano-TiO_2, sodium oleate and NS) with different SPs.

The length of the lateral chains varies as follows: PCE-D > PCE-C > PCE-A ≈ PCE-B (L. Dvorkin, N. Lushnikova, M. Sonebi, 2017). The best efficiency in NO removal of the mortars with PCE-C can be thus explained considering its better dispersion of the TiO_2 particles in the lime systems due to (i) its higher adsorption onto these particles, (ii) its highest anionic charge among the PCEs at the pH of the mortar and (iii) the noticeable length of its side chains (including 45 units of ethylene oxide) (Pérez-Nicolás et al., 2018).

In spite of having longer side chains (52 units), PCE-D showed lower adsorption and lower anionic charge, thus being not as effective as the PCE-C. The mortars with PCE-A and PCE-B showed similar NO abatement results due to the steric hindrance similarities. The highest adsorption of the PCE-A, mainly due to its lower molecular weight, resulted in a slightly faster stabilization of the nanoparticles.

These results were, in terms of dispersion of TiO_2, different from those reported in the work by Pérez-Nicolás et al. (Pérez-Nicolás et al., 2018), who confirmed a better dispersion of PCE-B and PCE-D. In the cited paper, the systems were aqueous coatings of TiO_2, whereas in the current work the SPs were added in bulk to a complex lime matrix, including nano-TiO_2, a water repellent, aggregate, lime particles and NS in some cases. There is agreement in the relatively poor performance of PNS: its working mechanism is not adequate for lime systems and due to its flat adsorption the growing

of hydration and carbonation compounds (deposits of calcium hydroxide, C-S-H, calcium carbonate) inactivates its dispersion ability (Pérez-Nicolás et al., 2018; Puertas et al., 2005).

The effect of the dosage of the superplasticizers was clear only for PCE-B and PCE-C, while for the others (PCE-A, PCE-D and PNS) there was not a clear dosage-response pattern. The complexity of the system, including different adsorption surfaces (lime particles, aggregate, TiO_2, in some cases nanosilica and the presence of oleate molecules) may explain this outcome (Plank and Winter, 2008).

Another outstanding issue considering the depolluting activity of these new mortars is the fact that the use of SPs also resulted in the enhancement of selectivity values (percentage ratio NO_x/NO), which were found to be 81.2% on average (Fig. 10).

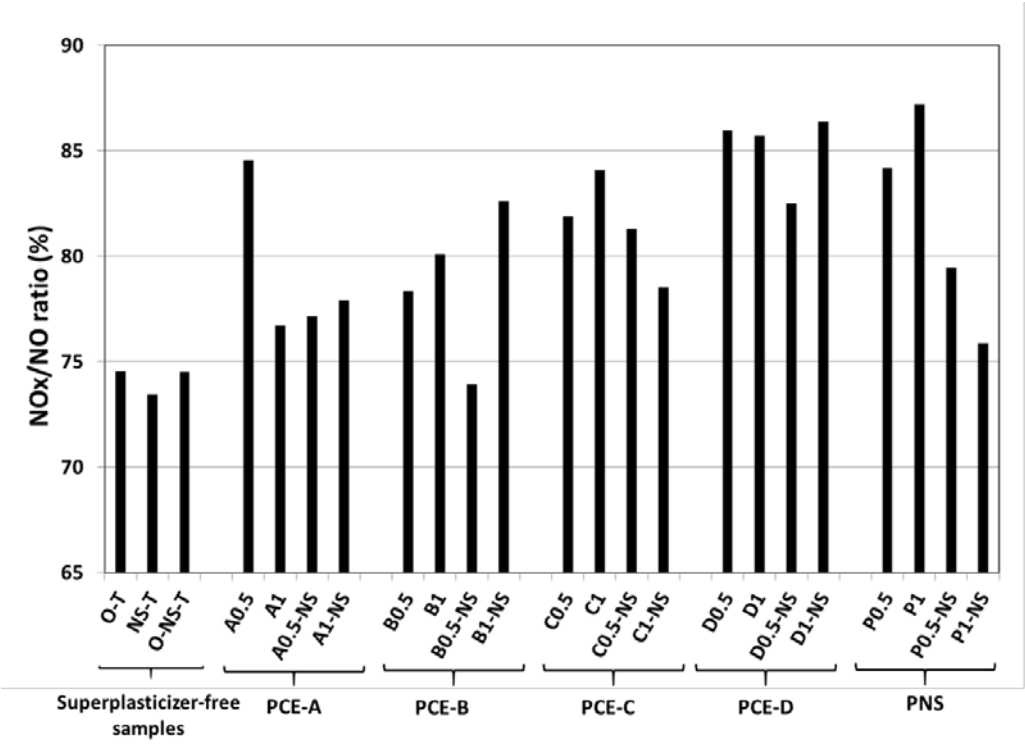

Fig. 10. Selectivity values (Percentage ratio NO_x/NO) of different samples

SP-free mortars yielded a mean value of 74.2% of selectivity, whereas a clear enhancement was seen for the mortars with the different SPs: 79.1% for PCE-A, 78.8% for PCE-B, 81.4% for PCE-C, 85.1% for PCE-D and 81.7% for PNS. From an environmental point of view, these results are relevant, since only a small fraction of the oxidized NO was released as NO_2 (a more dangerous and toxic pollutant) (Yang et al., 2019; Zouzelka and Rathousky, 2017). These selectivity values are close to the ones

achieved by new synthesized photocatalysts designed to reduce the NO_2 release (Yuan et al., 2020) and much higher than other selectivity values reported in the literature (Ambre et al., 2016; Balbuena et al., 2016; Luna et al., 2020). It must be highlighted that these high selectivity values were achieved in samples almost fully carbonated (see the values of the percentages of $CaCO_3$ obtained from the TG analyses in Table 2), which is a valuable result due to the reported decrease in selectivity as a consequence of the carbonation of either cement or lime (Kaja et al., 2019).

Table 2. Percentages of $CaCO_3$ (from TG results) in samples after 91 curing days.

Sample	$CaCO_3$ (%)
L	88.2
O-T	85.2
NS-T	87.3
O-NS-T	87.3
A0.5	90.4
A1	92.3
A0.5-NS	91.8
A1-NS	92.3
B0.5	92.5
B1	92.2
B0.5-NS	91.9
B1-NS	91.9
C0.5	91.8
C1	89.8
C0.5-NS	90.3
C1-NS	91.0
D0.5	88.0
D1	92.2
D0.5-NS	88.1
D1-NS	91.8
P0.5	87.7
P1	87.5
P0.5-NS	88.6
P1-NS	88.2

Two main reasons can be argued to explain the low release of NO_2. On the one hand, the chemical composition of the binding matrix. This composition includes the presence of alkaline-earth metallic ion (Ca^{2+}-rich system) that have been reported to adsorb NO_2 molecules (Papailias et al., 2018, 2017; Pérez-Nicolás et al., 2015) and, through a

chemisorption process onto calcium carbonate, give rise to the formation of nitrate (Lu et al., 2020); furthermore, the alkaline pH of the lime mortar matrix is able to allow the disproportionation of the NO_2 (Araña et al., 2019) and enhances the interaction with TiO_2, yielding an improvement of the photocatalytic performance (Jin et al., 2019). The increase in the surface adsorbed water, promoted by the alkaline hydrolysis of TiO_2 and by the hydrophilicity of the $Ca(OH)_2$ in this matrix, has been also reported to enhance the selectivity (Yang et al., 2018, 2017). On the other hand, the presence of SPs provides an effective TiO_2 separation, offering more possibilities for NO_2 adsorption and degradation onto TiO_2 particles (Sivachandiran et al., 2013). This was particularly significant to explain the differences with the free-SP mortars.

3.2. Self-cleaning effect and photoinduced hydrophilicity

3.2.1 Self-cleaning performance

The degradation of the dye deposited onto the surface of the mortars was studied as indicative of the self-cleaning ability of the mortars. In order to monitor the decoloring efficiency, each one the superficially stained mortars (mortars after 91 curing days) were compared with their bared counterparts and accordingly the influence of the porosity was to a certain extent attenuated. The discoloration along time under light exposure was recorded and expressed as ΔC_n (Fig. 11). The mortars without nano-TiO_2 were able to degrade the dye (Rhodamine B, RhB) up to ca. 44%. This result can be ascribed to the self-degradation of the dye (Fornasini et al., 2019), also fostered by the alkaline hydrolysis of the pigment (Zhan et al., 2000; Zhu et al., 2012) due to the alkaline conditions of the lime mortars. The TiO_2-free mortars were able to discolor the dye in values slightly higher to those reported for limestones (Fornasini et al., 2019) because of the latter aforementioned reason.

In the presence of the nano-TiO_2 admixture, the lime mortars were able to remove up to ca. 54% of the RhB over 310 minutes. The increase in the dye degradation (10%) and the final values were in line with previously reported self-cleaning abilities of TiO_2-bearing coatings (Fornasini et al., 2019). The role of the superplasticizers was also studied. The PCEs B, C and D enhanced the discoloration of the stained mortar, reaching degradation values close to 70% in many samples, and therefore increasing the self-cleaning ability of the lime mortars with respect to the SP-free specimens.

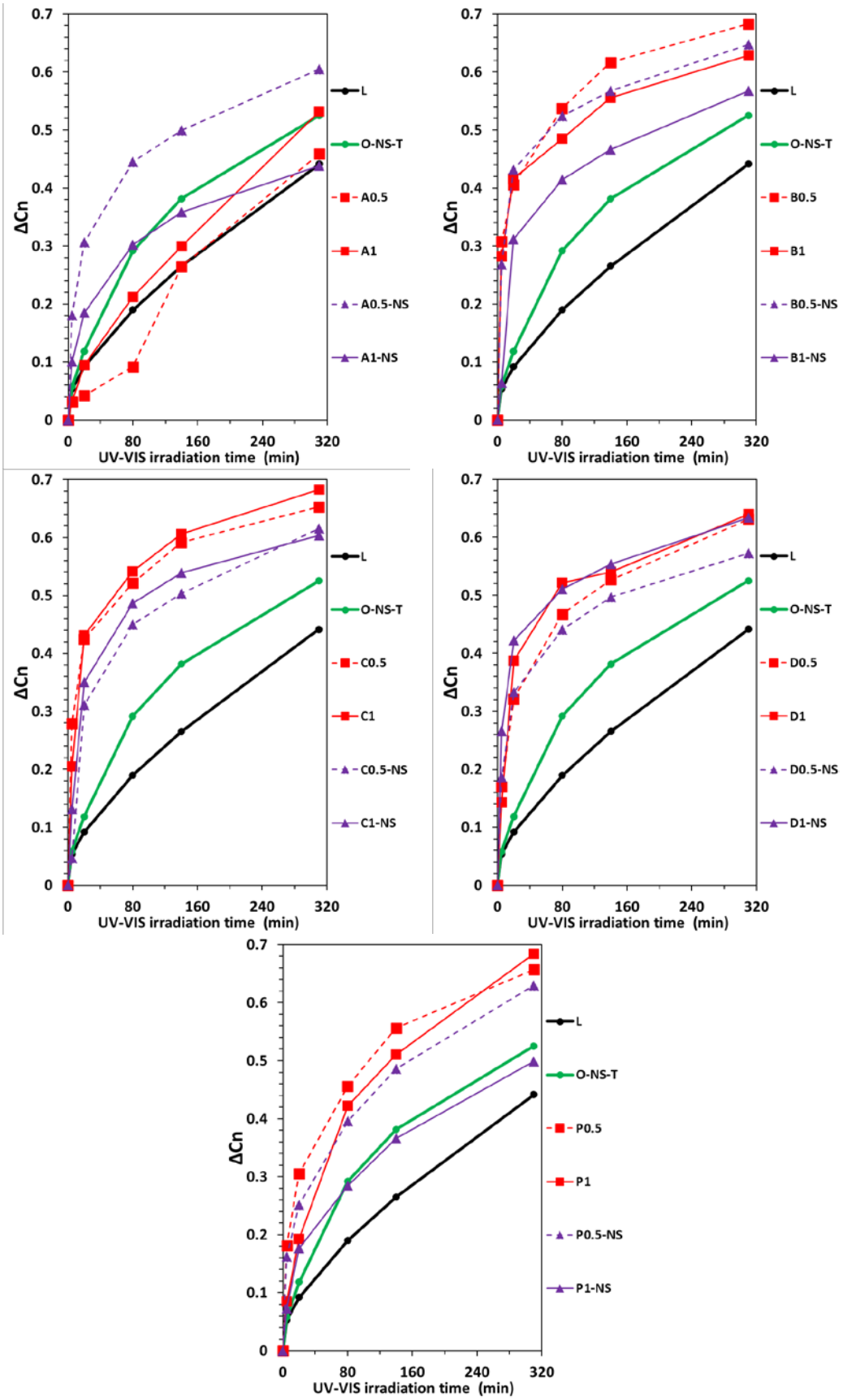

Fig. 11. Normalized chroma change (ΔC_n) (discoloration) for Rh-B stained samples at different UV-Vis exposure time.

In comparison with TiO_2-free mortars and SP-free mortars, respectively, PCE-B enhanced the decoloring efficiency 1.43 and 1.20 times on average; PCE-C, 1.45 and 1.22 times; and PCE-D 1.40 and 1.18 times. As in the case of the photocatalytic activity (NO abatements), the mortars with PCE-C yielded the highest efficiency, followed by PCE-B and PCE-D. The decomposition kinetics was also fast for these samples, yielding between 30 and 45% of dye degradation in just 20 minutes of illumination. Samples without SPs only reached 11% of discoloration in the same period of time.

Mortars with PNS also yielded dye degradation in the range of 60-70%, except for the poor performance of sample P1-NS (with just 50% of discoloration). It should be borne in mind that this sample also showed a low percentage of nitric oxide abatement (Fig. 2). These results can be attributed to the fact that this sample presented the lowest macroporosity (pores > 1 μm) among all the SP-bearing mortars. For the other samples with PNS, in comparison with the samples with PCEs B, C and D, the kinetics of the degradation was more sluggish. After 20 minutes of irradiation, only a 15% to 30% of the dye was degraded.

The PCE-A, in spite of yielding acceptable NO abatement results, did not show a good self-cleaning performance: only the mortar A0.5-NS was able to degrade up to 60% of RhB. The degradation kinetics for these samples was extremely sluggish (on average just 15% of degradation during the first 20 min of irradiation). The reasons for such performance are not easy to elucidate. Since the pore size distribution of these mortars was similar to the others with PCEs (Fig. 4) and the NO abatement was effective (Fig. 2), some interaction of the dye with the superplasticizer should be hypothesized as the cause of the poor self-cleaning performance. Under the UV-Vis irradiation, two ways of the Rhodamine B degradation can be expected (Ahmed et al., 2017; Bera et al., 2020; Lei et al., 2005; Rochkind et al., 2015): **1)** a photosensitization mechanism, in which the dye absorbs the visible light reaching the excited state. The excited dye then transfers charge to the conduction band of the semiconductor (TiO_2 in this case) and reactive $^{\bullet}OH$ radical is formed, which in its turn is responsible for the degradation of the dye molecule (Wu et al., 1998); **2)** a direct photocatalytic mechanism, in which upon absorption of the UV photons by the TiO_2, charge separation and formation of active species occur on the semiconductor, which will end up degrading the dye.

The second mechanism with TiO_2 only works under UV irradiation which energy matches the band-gap of the semiconductor, and understandably the NO abatement is also strictly dependent on it (Rochkind et al., 2015; Yu et al., 2014). However, if the first mechanism prevails, some interference during the charge donation from the dye to the semiconductor might block the dye degradation, and this reason can be postulated to explain the poor self-cleaning performance of the mortars with PCE-A.

In support of this argument, besides the similarities of the PCE-A mortars concerning the pore size distribution and the NO abatement, two additional considerations can be made: **i)** previous works have shown that the contribution of the visible light illumination to the dye degradation is higher than that of the UV light, irrespective of the intensity of the irradiation, remarking the significance of the photosensitization process in the decoloring efficiency (Kuo and Ho, 2001; Rochkind et al., 2015; Wu et al., 1998); **ii)** the experimental results show the differences in the kinetics of the degradation, being the PCE-A mortars the samples with the slowest degradation. With undoped TiO_2, the photosensitization has been confirmed to exhibit faster discoloration kinetics than that of the direct photocatalytic degradation (Rochkind et al., 2015), so that the later appears as prevalent in PCE-A mortars (slow kinetics), whereas the former is predominant in the others PCEs (fast kinetics) that present good self-cleaning performance.

The different adsorption of this polymer onto semiconductor particles and its low molecular weight might explain its favored interstitial arrangement between the adsorbed dye and the semiconductor, hindering the photosensitization mechanism of RhB degradation (Ojani et al., 2012).

3.2.2 Photoinduced hydrophilicity

In order to have a full understanding of the influence of the different admixtures in the self-cleaning performance of the lime mortars, the second approach of this research work was to study if the addition of the waterproofing admixture (sodium oleate) might interfere with that property. Specifically, the waterproofing agent could reduce the photoinduced hydrophilicity due to its water repelling action. The 91 days-aged lime mortars were thus exposed to irradiation and the static water contact angle (CA) was monitored at different times. Fig. 12 shows the different graphs of the surface wettability of the mortars for each one of the tested SPs.

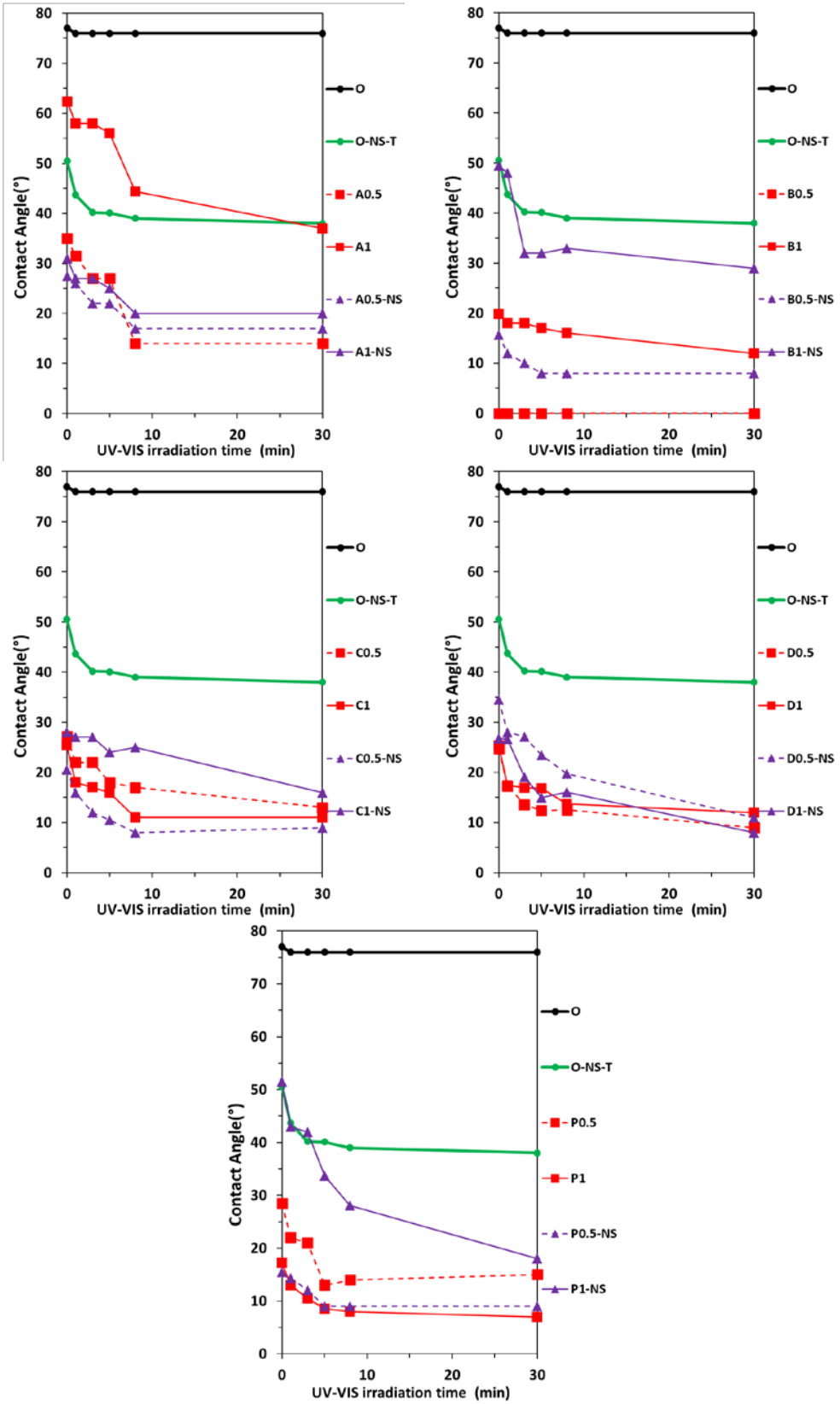

Fig. 12. Static water contact angle (CA) as a function of the UV-Vis irradiation time of different samples.

At time 0 min, before the irradiation, the sodium oleate reduced the wettability of the surface, with a high CA. Whilst the CA could not be determined for the control mortar

(admixture-free lime mortar) due to the instantaneous absorption of the water drop, the addition of sodium oleate (sample O) sharply increased the CA of the mortar (up to ca. 80º), proving the hydro-repellency imparted to the mortars by the oleate. The addition of other admixtures, such as NS and nano-TiO_2 increased the wettability of the mortars, because, among other reasons, the dilution effect of the oleate (owing to the addition of 20% and 2.5% of NS and TiO_2 by weight of lime). For example, in photocatalyst-bearing mortar O-NS-T, continuous irradiation for 30 minutes caused a CA moderate drop from 51º to 37º (i.e. a 27% of CA reduction).

The presence of the superplasticizers in the mortars induced noticeable changes in the CA values, proving their ability to favor the photoinduced hydrophilicity owing to the dispersion of TiO_2 active sites. CA values below 10º were obtained for some samples after 30 min of irradiation. The lowest CA values were achieved in mortars with PCE-D, PCE-C and PNS. On average, the percentages of CA reduction for samples before and after 30 minutes irradiation of UV-Vis light were ca. 44% for PCE-A and PCE-B, ca. 52% for PCE-C and PNS and ca. 64% for PCE-D.

Fig. 13 shows the profile of the water drops after deposition on the surface of different mortars after 3 minutes of irradiation, allowing observing the different wettability of the specimens.

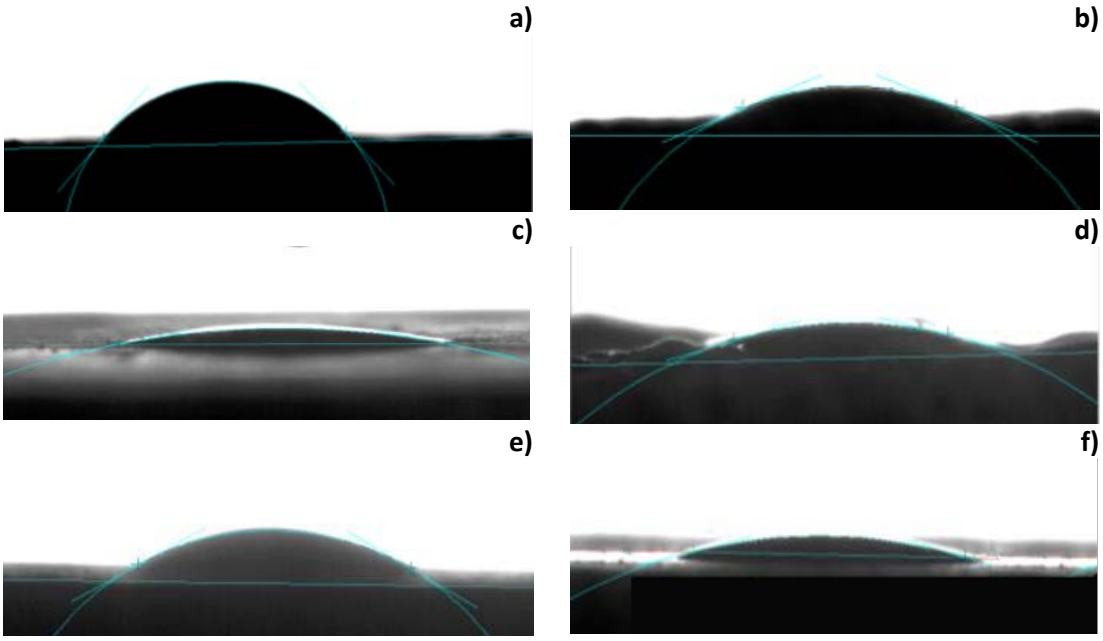

Fig. 13. Water droplets over different samples after 3 minutes of UV-Vis irradiation: (a) O-NS-T, (b) A0.5-NS, (c) B0.5-NS, (d) C0.5-NS, (e) D0.5-NS and (f) P0.5-NS.

These results are in line with previous results on photocatalytic coatings (Fornasini et al., 2019), and they confirm that the incorporation of superplasticizers in bulk allowed the preservation of the photoinduced hydrophilicity in these lime mortars, favoring their self-cleaning characteristics. It must be taken into account that the combined actions between hydrophobic agents and photocatalytic TiO_2 particles have been found to be complex in samples treated with coatings, needing for a balance between the reduction of the photoactivity and the hydrophobicity of the treated surface (La Russa et al., 2016; Scalarone et al. 2012; Cappelletti et al., 2015; Manoudis et al., 2009). In previous works, the addition of a waterproofing agent (sodium oleate in some cases) has been shown to increase the durability of the lime mortars (Atahan et al., 2008; Izaguirre et al., 2009; Izaguirre et al., 2010; Silva et al., 2020; González-Sánchez et al., 2021). Further works should address in optimized formulations the real effect of the waterproofing agent and the durability of the mortars. In this work, the presence of sodium oleate has been proved not to be detrimental for the photoinduced hydrophilicity and thus for the self-cleaning properties of the lime mortars.

4. Conclusions

1. The addition of superplasticizers resulted in a clear increase of the depolluting action of the lime mortars by 33% on average as compared with SP-free mortars, reaching a 44% of NO removal. In these mortars, a certain influence of the macropores > 1 μm was identified. The effective charge carrier separation was found to enhance the photoactivity, particularly for mortars with PCE-C as superplasticizer. The polycarboxylated SPs increased more the photoactivity than PNS and this was related to the molecular architecture of the SPs, which dominated the adsorption of the SPs, the anionic charge density and the length of the side chains of the PCEs.

2. NO_2 formation was hampered in a good degree due to the use of dispersing admixtures, which provided selectivity values as high as 87%. These good results were ascribed to the positive effect of the superplasticizers and to the characteristics of the lime matrix, with alkaline pH and alkaline-earth ions.

3. The self-cleaning ability of the mortars was also improved by the addition of SPs. The study of the degradation of the Rhodamine B dye deposited onto the surface of the mortars showed ca. 70% of discoloration after 310 minutes of UV-Vis irradiation With respect to TiO_2-free mortars, PCEs B, C and D enhanced the decoloring efficiency 1.43

times on average. With respect to SP-free TiO_2-bearing mortars, the enhancement of the self-cleaning ability was 1.20 times. The poor performance of PCE-A concerning the self-cleaning activity was related to the interference with the photosensitization mechanism of the dye degradation (dependent on the visible light excitation of the dye), which was found to be fostered by the other PCEs that displayed faster kinetics of degradation.

4. This study demonstrated that the presence of SPs also enhanced the photoinduced hydrophilicity of the mortars, a mechanism that favors the self-cleaning action. The presence of sodium oleate was compatible with the photoinduced wettability of the surface. Particularly PCE-D, PCE-C and PNS fostered the achievement of low CA values (ca. 10º) during the irradiation of the mortars.

5. PCE-C was overall the best dispersing admixture to enhance photocatalytic activity and self-cleaning ability of lime mortars. Further studies might be addressed to adjust the dosages and the water/lime ratio of these mortars depending on their final application as rendering mortars (one-coat, multilayer or repointing mortars). These future studies should also perform the assessment of the properties in hardened state, including those related to water absorption and transport phenomena, mechanical strengths, adherence and durability, as well as in situ real application and evaluation. These studies would allow to obtain interesting photocatalytically active and self-cleaning materials.

Funding

This study was funded by Spanish Ministry of Economy and Competitiveness (MINECO), grant number MAT2015-70728-P, and by the Government of Navarra, grant number PC142-143. The first author thanks the Friends of the University of Navarra, Inc., for a pre-doctoral grant.

Acknowledgments

The authors thank the technical support provided by Cristina Luzuriaga.

References

Ahmed, M.A., Abou-Gamra, Z.M., Medien, H.A.A., Hamza, M.A., 2017. Effect of porphyrin on photocatalytic activity of TiO_2 nanoparticles toward Rhodamine B photodegradation. J. Photochem. Photobiol. B Biol. 176, 25–35. https://doi.org/10.1016/j.jphotobiol.2017.09.016

Alvarez, J.I., Fernández, J.M., Navarro-Blasco, I., Duran, A., Sirera, R., 2013. Microstructural consequences of nanosilica addition on aerial lime binding materials: Influence of different drying conditions. Mater. Charact. 80, 36–49. https://doi.org/10.1016/j.matchar.2013.03.006

Ambre, R.B., Mane, S.B., Hung, C.H., 2016. Zinc porphyrins possessing three p-carboxyphenyl groups: Effect of the donor strength of push-groups on the efficiency of dye sensitized solar cells. Energies 9. https://doi.org/10.3390/en9070513

Ângelo, J., Andrade, L., Madeira, L.M., Mendes, A., 2013. An overview of photocatalysis phenomena applied to NO_x abatement. J. Environ. Manage. 129, 522–539. https://doi.org/10.1016/j.jenvman.2013.08.006

Araña, J., Garzón Sousa, D., González Díaz, O., Pulido Melián, E., Doña Rodríguez, J.M., 2019. Effect of NO_2 and NO_3-/HNO_3 adsorption on no photocatalytic conversion. Appl. Catal. B Environ. 244, 660–670. https://doi.org/10.1016/j.apcatb.2018.12.005

Arehart, J.H., Nelson, W.S., Srubar, W. V., 2020. On the theoretical carbon storage and carbon sequestration potential of hempcrete. J. Clean. Prod. 266. 121846 https://doi.org/10.1016/j.jclepro.2020.121846

Arrigoni, A., Pelosato, R., Melià, P., Ruggieri, G., Sabbadini, S., Dotelli, G., 2017. Life cycle assessment of natural building materials: the role of carbonation, mixture components and transport in the environmental impacts of hempcrete blocks. J. Clean. Prod. 149, 1051–1061. https://doi.org/10.1016/j.jclepro.2017.02.161

Atahan, H.N., Carlos, C., Chae, S., Monteiro, P.J.M., Bastacky, J., 2008. The morphology of entrained air voids in hardened cement paste generated with different anionic surfactants. Cem. Concr. Compos. 30, 566–575. https://doi.org/10.1016/j.cemconcomp.2008.02.003

Azeiteiro, L.C., Velosa, A., Paiva, H., Mantas, P.Q., Ferreira, V.M., Veiga, R., 2014. Development of grouts for consolidation of old renders. Constr. Build. Mater. 50, 352–360. https://doi.org/10.1016/j.conbuildmat.2013.09.006

Balbuena, J., Carraro, G., Cruz, M., Gasparotto, A., Maccato, C., Pastor, A., Sada, C., Barreca, D., Sánchez, L., 2016. Advances in photocatalytic NO_x abatement through the use of Fe_2O_3/TiO_2 nanocomposites. RSC Adv. 6, 74878–74885. https://doi.org/10.1039/c6ra15958c

Ballari, M.M. Brouwers, H.J.H., 2013. Full scale demonstration of air-purifying pavement, J. Hazard. Mater. 254–255, 406-414, https://doi.org/10.1016/j.jhazmat.2013.02.012.

Baltazar, L.G., Henriques, F.M.A., Jorne, F., Cidade, M.T., 2013. The use of rheology in the study of the composition effects on the fresh behaviour of hydraulic lime grouts for injection of masonry walls. Rheol. Acta 52, 127–138. https://doi.org/10.1007/s00397-013-0674-x

Bera, K.K., Chakraborty, M., Mondal, M., Banik, S., Bhattacharya, S.K., 2020. Synthesis of α-β Bi2O3 heterojunction photocatalyst and evaluation of reaction mechanism for degradation of RhB dye under natural sunlight. Ceram. Int. 46, 7667–7680. https://doi.org/10.1016/j.ceramint.2019.11.269

Bloh, J.Z., Folli, A., Macphee, D.E., 2014. Photocatalytic NO_x abatement: Why the selectivity matters. RSC Adv. 4, 45726–45734. https://doi.org/10.1039/c4ra07916g

Cappelletti, G. Fermo, P. Camiloni, M., 2015. Smart hybrid coatings for natural stones conservation, Prog. Org. Coat. 78, 511-516, https://doi.org/10.1016/j.porgcoat.2014.05.029.

Carmona-Quiroga, P.M. Martínez-Ramírez, S. Viles, H.A., 2018. Efficiency and durability of a self-cleaning coating on concrete and stones under both natural and artificial ageing trials, Appl. Surf. Sci. 433, 312-320, https://doi.org/10.1016/j.apsusc.2017.10.052.

Colangiuli, D. Calia, A. Bianco, N.. 2015. Novel multifunctional coatings with photocatalytic and hydrophobic properties for the preservation of the stone building heritage, Constr. Build. Mater. 93, 189-196, https://doi.org/10.1016/j.conbuildmat.2015.05.100.

Colangiuli, D. Lettieri, M. Masieri, M. Calia, A., 2019. Field study in an urban environment of simultaneous self-cleaning and hydrophobic nanosized TiO2-based coatings on stone for the protection of building surface, Sci. Total Environ. 650, 2919-2930, https://doi.org/10.1016/j.scitotenv.2018.10.044.

Corrêa, M.D.P., 2015. Solar ultraviolet radiation: Properties, characteristics and amounts observed in Brazil and south America. An. Bras. Dermatol. 90, 297–313. https://doi.org/10.1590/abd1806-4841.20154089

Crépy, L., Petit, J.Y., Wirquin, E., Martin, P., Joly, N., 2014. Synthesis and evaluation of starch-based polymers as potential dispersants in cement pastes and self leveling compounds. Cem. Concr. Compos. 45, 29–38. https://doi.org/10.1016/j.cemconcomp.2013.09.004

Crupi, V., Fazio, B., Gessini, A., Kis, Z., La Russa, M.F., Majolino, D., Masciovecchio, C., Ricca, M., Rossi, B., Ruffolo, S.A., Venuti, V., 2018. TiO_2–SiO_2–PDMS nanocomposite coating with self-cleaning effect for stone material: Finding the optimal amount of TiO_2. Constr. Build. Mater. 166, 464–471. https://doi.org/10.1016/j.conbuildmat.2018.01.172

Dalton, J.S., Janes, P.A., Jones, N.G., Nicholson, J.A., Hallam, K.R., Allen, G.C., 2002. Photocatalytic oxidation of NO_x gases using TiO_2: A surface spectroscopic approach. Environ. Pollut. 120, 415–422. https://doi.org/10.1016/S0269-7491(02)00107-0

Deng, X., Li, J., Lu, Z., Chen, J., Luo, K., Niu, Y., 2020. Effect of hydrated lime on structures and properties of decorative rendering mortar. Constr. Build. Mater. 256. 119485 https://doi.org/10.1016/j.conbuildmat.2020.119485

Diamanti, M.V. Paolini, R., Rossini, M., Aslan, A.B., Zinzi, M., Poli, T., Pedeferri, M.P., 2015. Long term self-cleaning and photocatalytic performance of anatase added mortars exposed to the urban environment, Constr. Build. Mater. 96, 270-278, https://doi.org/10.1016/j.conbuildmat.2015.08.028.

Draft International Standard, 2007. Fine ceramics (advanced ceramics , advanced technical ceramics) — Test method for air-purification performance of semiconducting photocatalytic materials — Part 1 : Removal of nitric oxide [WWW Document]. Draft Int. Stand. URL http://www.iso.org/iso/home/store/catalogue_tc/catalogue_detail.htm?csnumber=40761

Duran, A., González-Sánchez, J.F., Fernández, J.M., Sirera, R., Navarro-Blasco, Í., Alvarez, J.I., 2018. Influence of two polymer-based superplasticizers (poly-naphthalene sulfonate, PNS, and lignosulfonate, LS) on compressive and flexural strength, freeze-thaw, and sulphate attack resistance of lime-metakaolin grouts. Polymers (Basel). 10. https://doi.org/10.3390/polym10080824

Duran, A., Navarro-Blasco, I., Fernández, J.M., Alvarez, J.I., 2014. Long-term mechanical resistance and durability of air lime mortars with large additions of nanosilica. Constr. Build. Mater. 58, 147–158. https://doi.org/10.1016/j.conbuildmat.2014.02.030

Dvorkin, L., Lushnikova, N., Sonebi, M., Khatib, J., 2017. Properties of modified phosphogypsum binder. Academic Journal of Civil Engineering, 35(2), 96-102. https://doi.org/10.26168/icbbm2017.13.

European Committee for Standardization, 1999a. UNE-EN 1015-6:1999 Methods of Test for Mortar for Masonry. Part 6: Determination of Bulk Density of Fresh Mortar. EN.

European Committee for Standardization, 1999b. UNE-EN 1015-9:1999 Methods of Test for Mortar for Masonry, Part 9: Determination of Workable Life and Correction Time of Fresh Mortar. EN.

European Committee for Standardization, 1999c. UNE-EN 1015-7:1999 Methods of Test for Mortar for Masonry. Part 7: Determination of Air Content of Fresh Mortar. EN.

European Committee for Standardization, 2005. UNE-EN 196-1 Methods of testing cement. Part 1: Determination of strength. EN.

European Committee for Standardization, 2006. UNE-EN 1015-3:2000 Methods of test for mortar for masonry —Part 3: Determination of consistence of fresh mortar (by flow table). EN.

European Committee for Standardization, 2016. EN 998-1:2016 Specification for mortar for masonry. Rendering and plastering mortar. EN.

Falchi, L., Müller, U., Fontana, P., Izzo, F.C., Zendri, E., 2013. Influence and effectiveness of water-repellent admixtures on pozzolana-lime mortars for restoration application. Constr. Build. Mater. 49, 272–280. https://doi.org/10.1016/j.conbuildmat.2013.08.030

Falchi, L., Zendri, E., Müller, U., Fontana, P., 2015. The influence of water-repellent admixtures on the behaviour and the effectiveness of Portland limestone cement mortars. Cem. Concr. Compos. 59, 107–118. https://doi.org/10.1016/j.cemconcomp.2015.02.004

Fediuk, R., Timokhin, R., Mochalov, A., Otsokov, K., Lashina, I., 2019. Performance properties of high-density impermeable cementitious paste. J. Mater. Civ. Eng. 31. 04019013 https://doi.org/10.1061/(ASCE)MT.1943-5533.0002633

Fernández, J.M., Duran, A., Navarro-Blasco, I., Lanas, J., Sirera, R., Alvarez, J.I., 2013. Influence of nanosilica and a polycarboxylate ether superplasticizer on the performance of lime mortars. Cem. Concr. Res. 43, 12–24. https://doi.org/10.1016/j.cemconres.2012.10.007

Folli, A., Pade, C., Hansen, T.B., De Marco, T., MacPhee, D.E., 2012. TiO_2 photocatalysis in cementitious systems: Insights into self-cleaning and depollution chemistry. Cem. Concr. Res. 42, 539–548. https://doi.org/10.1016/j.cemconres.2011.12.001

Fornasini, L., Bergamonti, L., Bondioli, F., Bersani, D., Lazzarini, L., Paz, Y., Lottici, P.P., 2019. Photocatalytic N-doped TiO_2 for self-cleaning of limestones. Eur. Phys. J. Plus 134, 539. https://doi.org/10.1140/epjp/i2019-12981-6

Gandolfo, A., Bartolomei, V., Gomez Alvarez, E., Tlili, S., Gligorovski, S., Kleffmann, J., Wortham, H., 2015. The effectiveness of indoor photocatalytic paints on NO_x and HONO levels. Appl. Catal. B Environ. 166–167, 84–90. https://doi.org/10.1016/j.apcatb.2014.11.011

Giosuè, C., Mobili, A., Citterio, B., Biavasco, F., Ruello, M.L., Tittarelli, F., 2020. Innovative hydraulic lime-based finishes with unconventional aggregates and TiO_2 for the improvement of indoor air quality. Manuf. Rev. 7. https://doi.org/10.1051/mfreview/2020010

Giosuè, C., Yu, Q.L., Ruello, M.L., Tittarelli, F., Brouwers, H.J.H., 2018. Effect of pore structure on the performance of photocatalytic lightweight lime-based finishing mortar. Constr. Build. Mater. 171, 232–242. https://doi.org/10.1016/j.conbuildmat.2018.03.106

González-Sánchez, J.F. Fernández, J.M. Navarro-Blasco, Í. Alvarez, J.I., 2021. Improving lime-based rendering mortars with admixtures, Constr. Build. Mater. 271, 121887, https://doi.org/10.1016/j.conbuildmat.2020.121887.

González-Sánchez, J.F., Taşci, B., Fernández, J.M., Navarro-Blasco, Í., Alvarez, J.I., 2020. Combination of polymeric superplasticizers, water repellents and pozzolanic agents to improve air lime-based grouts for historic masonry repair. Polymers (Basel). 12. https://doi.org/10.3390/POLYM12040887

Guerrini, G.L., 2012, Photocatalytic performances in a city tunnel in Rome: NOx monitoring results, Constr. Build. Mater. 27, 165-175. https://doi.org/10.1016/j.conbuildmat.2011.07.065.

Guo, M.Z., Maury-Ramirez, A., Poon, C.S., 2016. Self-cleaning ability of titanium dioxide clear paint coated architectural mortar and its potential in field application, J. Clean. Prod. 112, 3583-3588, https://doi.org/10.1016/j.jclepro.2015.10.079.

Haider, A.J., Jameel, Z.N., Al-Hussaini, I.H.M., 2019. Review on: Titanium dioxide applications, in: Energy Procedia. Elsevier Ltd, pp. 17–29. https://doi.org/10.1016/j.egypro.2018.11.159

Heikkilä, A., Kärhä, P., Tanskanen, A., Kaunismaa, M., Koskela, T., Kaurola, J., Ture, T., Syrjälä, S., 2009. Characterizing a UV chamber with mercury lamps for assessment of comparability to natural UV conditions. Polym. Test. 28, 57–65. https://doi.org/10.1016/j.polymertesting.2008.10.005

Izaguirre, A., Lanas, J., Álvarez, J.I., 2009. Effect of water-repellent admixtures on the behaviour of aerial lime-based mortars. Cem. Concr. Res. 39, 1095–1104. https://doi.org/10.1016/J.CEMCONRES.2009.07.026

Izaguirre, A., Lanas, J., Álvarez, J.I., 2010. Ageing of lime mortars with admixtures: Durability and strength assessment. Cem. Concr. Res. 40, 1081–1095. https://doi.org/10.1016/j.cemconres.2010.02.013

Izaguirre, A., Lanas, J., Álvarez, J.I., 2011. Characterization of aerial lime-based mortars modified by the addition of two different water-retaining agents. Cem. Concr. Compos. 33, 309–318. https://doi.org/10.1016/j.cemconcomp.2010.09.008

Jiménez-Relinque, E. J.R. Rodriguez-Garcia, J.R. A. Castillo, A. Castellote, M., 2015. Characteristics and efficiency of photocatalytic cementitious materials: Type of binder, roughness and microstructure, Cem. Concr. Res. 71, 124-131.,

Jin, Q., Saad, E.M., Zhang, W., Tang, Y., Kurtis, K.E., 2019. Quantification of NO_x uptake in plain and TiO_2-doped cementitious materials. Cem. Concr. Res. 122, 251–256. https://doi.org/10.1016/j.cemconres.2019.05.010

Kaja, A.M., Brouwers, H.J.H., Yu, Q.L., 2019. NO_x degradation by photocatalytic mortars: The underlying role of the CH and C-S-H carbonation. Cem. Concr. Res. 125. https://doi.org/10.1016/j.cemconres.2019.105805

Kapridaki, C., Verganelaki, A., Dimitriadou, P., Maravelaki-Kalaitzaki, P., 2018. Conservation of monuments by a three-layered compatible treatment of TEOS-Nano-Calcium Oxalate consolidant and TEOS-PDMS-TiO_2 hydrophobic/photoactive hybrid nanomaterials. Materials (Basel). 11. https://doi.org/10.3390/ma11050684

Kapridaki, C., Xynidis, N., Vazgiouraki, E., Kallithrakas-Kontos, N., Maravelaki-Kalaitzaki, P., 2019. Characterization of photoactive Fe-TiO_2 lime coatings for building protection: The role of Iron content. Materials (Basel). 12. https://doi.org/10.3390/ma12111847

Krishnan, P., Zhang, M.H., Yu, L.E., 2018. Removal of black carbon using photocatalytic silicate-based coating: Laboratory and field studies. J. Clean. Prod. 183, 436–448. https://doi.org/10.1016/j.jclepro.2018.02.149

Krou, N.J., Batonneau-Gener, I., Belin, T., Mignard, S., Horgnies, M., Dubois-Brugger, I., 2013. Mechanisms of NO_x entrapment into hydrated cement paste containing activated carbon - Influences of the temperature and carbonation. Cem. Concr. Res. 53, 51–58. https://doi.org/10.1016/j.cemconres.2013.06.006

Kuo, W.S., Ho, P.H., 2001. Solar photocatalytic decolorization of methylene blue in water. Chemosphere 45, 77–83. https://doi.org/10.1016/S0045-6535(01)00008-X

La Russa, M.F. Rovella, N. Alvarez de Buergo, M. Belfiore, C.M. Pezzino, A. Crisci, G.M. Ruffolo, S.A., 2016. Nano-TiO2 coatings for cultural heritage protection: The role of the binder on hydrophobic and self-cleaning efficacy, Prog. Org. Coat. 91, 1-8, https://doi.org/10.1016/j.porgcoat.2015.11.011.

Lanas, J., Alvarez, J.I., 2003. Masonry repair lime-based mortars: Factors affecting the mechanical behavior. Cem. Concr. Res. 33, 1867–1876. https://doi.org/10.1016/S0008-8846(03)00210-2

Lei, P., Chen, C., Yang, J., Ma, W., Zhao, J., Zang, L., 2005. Degradation of dye pollutants by immobilized polyoxometalate with H_2O_2 under visible-light irradiation. Environ. Sci. Technol. 39, 8466–8474. https://doi.org/10.1021/es050321g

Lettieri, M., Colangiuli, D., Masieri, M., Calia, A., 2019. Field performances of nanosized TiO2 coated limestone for a self-cleaning building surface in an urban

environment, Build. Environ. 147, 506-516, https://doi.org/10.1016/j.buildenv.2018.10.037.

Liao, D.L., Wu, G.S., Liao, B.Q., 2009. Zeta potential of shape-controlled TiO_2 nanoparticles with surfactants. Colloids Surfaces A Physicochem. Eng. Asp. 348, 270–275. https://doi.org/10.1016/j.colsurfa.2009.07.036

Liufu, S., Xiao, H., Li, Y., 2005. Adsorption of poly(acrylic acid) onto the surface of titanium dioxide and the colloidal stability of aqueous suspension. J. Colloid Interface Sci. 281, 155–163. https://doi.org/10.1016/j.jcis.2004.08.075

Lu, Z.Z., Li, S.Q., Xiao, J.Y., 2020. Synergetic Effect of Na–Ca for Enhanced Photocatalytic Performance in NO_x Degradation by g-C_3N_4. Catal. Lett. https://doi.org/10.1007/s10562-020-03318-5

Lucas, S.S., Ferreira, V.M., De Aguiar, J.L.B., 2013. Incorporation of titanium dioxide nanoparticles in mortars - Influence of microstructure in the hardened state properties and photocatalytic activity. Cem. Concr. Res. 43, 112–120. https://doi.org/10.1016/j.cemconres.2012.09.007

Luna, M., Gatica, J.M., Vidal, H., Mosquera, M.J., 2020. Use of Au/N-TiO_2/SiO_2 photocatalysts in building materials with NO depolluting activity. J. Clean. Prod. 243, 118633. https://doi.org/10.1016/j.jclepro.2019.118633

Luna, M., Mosquera, M.J., Vidal, H., Gatica, J.M., 2019. Au-TiO_2/SiO_2 photocatalysts for building materials: Self-cleaning and de-polluting performance. Build. Environ. 164, 106347. https://doi.org/10.1016/j.buildenv.2019.106347

Magalhães, A. Veiga, R., 2009. Physical and mechanical characterisation of historic mortars. Application to the evaluation of the state of conservation Mater Construcc 59, 61-77, https://doi.org/10.3989/mc.2009.41907

Mamaghani, A.H., Haghighat, F., Lee, C.S., 2017. Photocatalytic oxidation technology for indoor environment air purification: The state-of-the-art. Appl. Catal. B Environ. 203, 247–269. https://doi.org/10.1016/j.apcatb.2016.10.037

Manoudis, P.N., Karapanagiotis, I., Tsakalof, A. et al. 2009. Superhydrophobic films for the protection of outdoor cultural heritage assets. Appl. Phys. A 97, 351–360, https://doi.org/10.1007/s00339-009-5233-z

Martínez-García, C., González-Fonteboa, B., Carro-López, D., Martínez-Abella, F., 2019. Impact of mussel shell aggregates on air lime mortars. Pore structure and carbonation. J. Clean. Prod. 215, 650–668. https://doi.org/10.1016/j.jclepro.2019.01.121

Mezhov, A., Ulka, S., Gendel, Y., Diesendruck, C.E., Kovler, K., 2020. The working mechanisms of low molecular weight polynaphthalene sulfonate superplasticizers.

Constr. Build. Mater. 240, 117891. https://doi.org/10.1016/j.conbuildmat.2019.117891

Munafò, P., Goffredo, G.B., Quagliarini, E., 2015. TiO_2-based nanocoatings for preserving architectural stone surfaces: An overview. Constr. Build. Mater. 84, 201-218.https://doi.org/10.1016/j.conbuildmat.2015.02.083

Navarro-Blasco, I., Pérez-Nicolás, M., Fernández, J.M., Duran, A., Sirera, R., Alvarez, J.I., 2014. Assessment of the interaction of polycarboxylate superplasticizers in hydrated lime pastes modified with nanosilica or metakaolin as pozzolanic reactives. Constr. Build. Mater. 73, 1–12. https://doi.org/10.1016/j.conbuildmat.2014.09.052

Nunes, C., Slížková, Z., 2016. Freezing and thawing resistance of aerial lime mortar with metakaolin and a traditional water-repellent admixture. Constr. Build. Mater. 114, 896–905. https://doi.org/10.1016/j.conbuildmat.2016.04.029

Nunes, C., Slížková, Z., Stefanidou, M., Němeček, J., 2016. Microstructure of lime and lime-pozzolana pastes with nanosilica. Cem. Concr. Res. 83, 152–163. https://doi.org/10.1016/j.cemconres.2016.02.004

Ojani, R., Raoof, J.B., Zarei, E., 2012. Electrochemical monitoring of photoelectrocatalytic degradation of rhodamine B using TiO_2 thin film modified graphite electrode. J. Solid State Electrochem. 16, 2143–2149. https://doi.org/10.1007/s10008-011-1634-y

Orsini, F., Marrone, P., 2019. Approaches for a low-carbon production of building materials: A review. J. Clean. Prod. 241, 118380 https://doi.org/10.1016/j.jclepro.2019.118380

Padovnik, A., Bokan-Bosiljkov, V., 2020. Effect of ultralight filler on the properties of hydrated lime injection grout for the consolidation of detached historic decorative plasters. Materials (Basel). 13. https://doi.org/10.3390/ma13153360

Padovnik, A., Piqué, F., Jornet, A., Bokan-Bosiljkov, V., 2016. Injection Grouts for the Re-Attachment of Architectural Surfaces with Historic Value—Measures to Improve the Properties of Hydrated Lime Grouts in Slovenia. Int. J. Archit. Herit. 10, 993–1007. https://doi.org/10.1080/15583058.2016.1177747

Papailias, I., Todorova, N., Giannakopoulou, T., Karapati, S., Boukos, N., Dimotikali, D., Trapalis, C., 2018. Enhanced NO 2 abatement by alkaline-earth modified g-C 3 N 4 nanocomposites for efficient air purification. Appl. Surf. Sci. 430, 225–233. https://doi.org/10.1016/j.apsusc.2017.08.084

Papailias, I., Todorova, N., Giannakopoulou, T., Yu, J., Dimotikali, D., Trapalis, C., 2017. Photocatalytic activity of modified g-C3N4/TiO_2 nanocomposites for NO_x removal. Catal. Today 280, 37–44. https://doi.org/10.1016/j.cattod.2016.06.032

Pérez-Nicolás, M., Balbuena, J., Cruz-Yusta, M., Sánchez, L., Navarro-Blasco, I., Fernández, J.M., Alvarez, J.I., 2015. Photocatalytic NO_x abatement by calcium aluminate cements modified with TiO_2: Improved NO_2 conversion. Cem. Concr. Res. 70, 67–76. https://doi.org/10.1016/j.cemconres.2015.01.011

Pérez-Nicolás, M., Duran, A., Navarro-Blasco, I., Fernández, J.M., Sirera, R., Alvarez, J.I., 2016. Study on the effectiveness of PNS and LS superplasticizers in air lime-based mortars. Cem. Concr. Res. 82, 11–22. https://doi.org/10.1016/j.cemconres.2015.12.006

Pérez-Nicolás, M., Navarro-Blasco, Í., Fernández, J.M., Alvarez, J.I., 2017. The effect of TiO_2 doped photocatalytic nano-additives on the hydration and microstructure of portland and high alumina cements. Nanomaterials 7, 7100329. https://doi.org/10.3390/nano7100329

Pérez-Nicolás, M., Plank, J., Ruiz-Izuriaga, D., Navarro-Blasco, I., Fernández, J.M., Alvarez, J.I., 2018. Photocatalytically active coatings for cement and air lime mortars: Enhancement of the activity by incorporation of superplasticizers. Constr. Build. Mater. 162, 628–648. https://doi.org/10.1016/j.conbuildmat.2017.12.087

Plank, J., Winter, C., 2008. Competitive adsorption between superplasticizer and retarder molecules on mineral binder surface. Cem. Concr. Res. 38, 599–605. https://doi.org/10.1016/j.cemconres.2007.12.003

Plank, J., Yu, B., 2010. Preparation of hydrocalumite-based nanocomposites using polycarboxylate comb polymers possessing high grafting density as interlayer spacers. Appl. Clay Sci. 47, 378–383. https://doi.org/10.1016/j.clay.2009.11.057

Pozo-Antonio, J.S., Dionísio, A., 2017. Self-cleaning property of mortars with TiO_2 addition using real diesel exhaust soot. J. Clean. Prod. 161, 850–859. https://doi.org/10.1016/j.jclepro.2017.05.202

Prieto, C., Lagaron, J.M., 2020. Nanodroplets of docosahexaenoic acid-enriched algae oil encapsulated within microparticles of hydrocolloids by emulsion electrospraying assisted by pressurized gas. Nanomaterials 10. https://doi.org/10.3390/nano10020270

Puertas, F., Santos, H., Palacios, M., Martínez-Ramírez, S., 2005. Polycarboxylate superplasticiser admixtures: Effect on hydration, microstructure and rheological behaviour in cement pastes. Adv. Cem. Res. 17, 77–89. https://doi.org/10.1680/adcr.2005.17.2.77

Rochkind, M., Pasternak, S., Paz, Y., 2015. Using dyes for evaluating photocatalytic properties: A critical review. Molecules 20, 88–110. https://doi.org/10.3390/molecules20010088

Ruot, B., Plassais, A., Olive, F., Guillot, L., Bonafous, L., 2009. TiO_2-containing cement pastes and mortars: Measurements of the photocatalytic efficiency using a rhodamine B-based colourimetric test. Sol. Energy 83, 1794–1801. https://doi.org/10.1016/j.solener.2009.05.017

Saeli, M., Piccirillo, C., Tobaldi, D.M., Binions, R., Castro, P.M.L., Pullar, R.C., 2018. A sustainable replacement for TiO_2 in photocatalyst construction materials: Hydroxyapatite-based photocatalytic additives, made from the valorisation of food wastes of marine origin. J. Clean. Prod. 193, 115–127. https://doi.org/10.1016/j.jclepro.2018.05.030

Salavessa, E., Jalali, S., Sousa, L.M.O., Fernandes, L., Duarte, A.M., 2013. Historical plasterwork techniques inspire new formulations. Constr. Build. Mater. 48, 858–867. https://doi.org/10.1016/j.conbuildmat.2013.07.064

Santos, A.R., Veiga, M. do R., Santos Silva, A., de Brito, J., Álvarez, J.I., 2018. Evolution of the microstructure of lime based mortars and influence on the mechanical behaviour: The role of the aggregates. Constr. Build. Mater. 187, 907–922. https://doi.org/10.1016/j.conbuildmat.2018.07.223

Scalarone, D., Lazzari, M., Chiantore, O., 2012. Acrylic protective coatings modified with titanium dioxide nanoparticles: Comparative study of stability under irradiation, Polym. Degrad. Stab. 97, 2136-2142, https://doi.org/10.1016/j.polymdegradstab.2012.08.014.

Seabra, M.P., Labrincha, J.A., Ferreira, V.M., 2007. Rheological behaviour of hydraulic lime-based mortars. J. Eur. Ceram. Soc. 27, 1735–1741. https://doi.org/10.1016/j.jeurceramsoc.2006.04.155

Sharma, U., Singh, L.P., Zhan, B., Poon, C.S., 2019. Effect of particle size of nanosilica on microstructure of C-S-H and its impact on mechanical strength. Cem. Concr. Compos. 97, 312–321. https://doi.org/10.1016/j.cemconcomp.2019.01.007

Silva, B., Ferreira Pinto, A.P., Gomes, A., Candeias, A., 2019. Fresh and hardened state behaviour of aerial lime mortars with superplasticizer. Constr. Build. Mater. 225, 1127–1139. https://doi.org/10.1016/j.conbuildmat.2019.07.275

Silva, B.A., Ferreira Pinto, A.P., Gomes, A., Candeias, A., 2020. Comparative analysis of the behaviour of integral water-repellents on lime mortars. Constr. Build. Mater. 261, 120344. https://doi.org/10.1016/j.conbuildmat.2020.120344

Sivachandiran, L., Thevenet, F., Gravejat, P., Rousseau, A., 2013. Investigation of NO and NO_2 adsorption mechanisms on TiO_2 at room temperature. Appl. Catal. B Environ. 142–143, 196–204. https://doi.org/10.1016/j.apcatb.2013.04.073

Son, J., Kundu, S., Verma, L.K., Sakhuja, M., Danner, A.J., Bhatia, C.S., Yang, H., 2012. A practical superhydrophilic self cleaning and antireflective surface for

outdoor photovoltaic applications. Sol. Energy Mater. Sol. Cells 98, 46–51. https://doi.org/10.1016/j.solmat.2011.10.011

Strini, A. Cassese, S. Schiavi L., 2005. Measurement of benzene, toluene, ethylbenzene and o-xylene gas phase photodegradation by titanium dioxide dispersed in cementitious materials using a mixed flow reactor, Appl. Catal. B Environ. Applied Catalysis B: Environmental, Volume 61, Issues 1–2, 2005, Pages 90-97.

Sugrañez, R., Álvarez, J.I., Cruz-Yusta, M., Mármol, I., Morales, J., Vila, J., Sánchez, L., 2013. Enhanced photocatalytic degradation of NO_x gases by regulating the microstructure of mortar cement modified with titanium dioxide. Build. Environ. 69, 55–63. https://doi.org/10.1016/j.buildenv.2013.07.014

Tsardaka, E., Stefanidou, M., 2020. The Effects of Single and Combined Nanoparticles in the Properties of Air Lime Pastes. Int. J. Archit. Herit. 14, 964–976. https://doi.org/10.1080/15583058.2019.1703152

Veiga, M.R. Fragata, A. Velosa, A.L. Magalhães, A.C. Margalha, G., 2010. Lime-Based Mortars: Viability for Use as Substitution Renders in Historical Buildings, Int. J. Archit. Heritage, 4, 177-195, https://doi.org/10.1080/15583050902914678 julio-septiembre 2009

Walker, R., Pavía, S., 2014. Moisture transfer and thermal properties of hemp-lime concretes. Constr. Build. Mater. 64, 270–276. https://doi.org/10.1016/j.conbuildmat.2014.04.081

Wang, Z., Yu, Q., Gauvin, F., Feng, P., Qianping, R., Brouwers, H.J.H., 2020. Nanodispersed TiO_2 hydrosol modified Portland cement paste: The underlying role of hydration on self-cleaning mechanisms. Cem. Concr. Res. 136, 106156. https://doi.org/10.1016/j.cemconres.2020.106156

Wu, T., Liu, G., Zhao, J., Hidaka, H., Serpone, N., 1998. Photoassisted degradation of dye pollutants. V. Self-photosensitized oxidative transformation of Rhodamine B under visible light irradiation in aqueous TiO_2 dispersions. J. Phys. Chem. B 102, 5845–5851. https://doi.org/10.1021/jp980922c

Xia, T., Chen, W., Xu, J., 2020. Effect of PEG loading on the rheological stability of bitumen/PE/PEG blends based on network structure evolution. Constr. Build. Mater. 237, 117696. https://doi.org/10.1016/j.conbuildmat.2019.117696

Yang, L., Hakki, A., Wang, F., Macphee, D.E., 2017. Different Roles of Water in Photocatalytic $DeNO_x$ Mechanisms on TiO_2: Basis for Engineering Nitrate Selectivity? ACS Appl. Mater. Interfaces 9, 17034–17041. https://doi.org/10.1021/acsami.7b01989

Yang, L., Hakki, A., Wang, F., Macphee, D.E., 2018. Photocatalyst efficiencies in concrete technology: The effect of photocatalyst placement. Appl. Catal. B Environ. 222, 200–208. https://doi.org/10.1016/j.apcatb.2017.10.013

Yang, L., Hakki, A., Zheng, L., Jones, M.R., Wang, F., Macphee, D.E., 2019. Photocatalytic concrete for NO_x abatement: Supported TiO_2 efficiencies and impacts. Cem. Concr. Res. 116, 57–64. https://doi.org/10.1016/j.cemconres.2018.11.002

Yoshioka, K., Sakai, E., Daimon, M., Kitahara, A., 1997. Role of steric hindrance in the performance of superplasticizers for concrete. J. Am. Ceram. Soc. 80, 2667–2671. https://doi.org/10.1111/j.1151-2916.1997.tb03169.x

Yu, W., Liu, X., Pan, L., Li, J., Liu, J., Zhang, J., Li, P., Chen, C., Sun, Z., 2014. Enhanced visible light photocatalytic degradation of methylene blue by F-doped TiO_2. Appl. Surf. Sci. 319, 107–112. https://doi.org/10.1016/j.apsusc.2014.07.038

Yuan, C., Chen, R., Wang, J., Wu, H., Sheng, J., Dong, F., Sun, Y., 2020. La-doping induced localized excess electrons on $(BiO)_2CO_3$ for efficient photocatalytic NO removal and toxic intermediates suppression. J. Hazard. Mater. 400, 123174. https://doi.org/10.1016/j.jhazmat.2020.123174

Zhan, C.G., Landry, D.W., Ornstein, R.L., 2000. Reaction pathways and energy barriers for alkaline hydrolysis of carboxylic acid esters in water studied by a hybrid supermolecule-polarizable continuum approach. J. Am. Chem. Soc. 122, 2621–2627. https://doi.org/10.1021/ja9937932

Zhang, X., Tong, H., Zhang, H., Chen, C., 2008. Nitrogen oxides absorption on calcium hydroxide at low temperature. Ind. Eng. Chem. Res. 47, 3827–3833. https://doi.org/10.1021/ie070660d

Zhang, Y., Kong, X., 2015. Correlations of the dispersing capability of NSF and PCE types of superplasticizer and their impacts on cement hydration with the adsorption in fresh cement pastes. Cem. Concr. Res. 69, 1–9. https://doi.org/10.1016/j.cemconres.2014.11.009

Zhu, J., Shu, L., Zhang, F., Li, Z., Wang, Q., He, P., Fang, Y., 2012. Development of a compact capillary electrophoresis-chemiluminescence system with ultra-fast peroxyoxalate reaction to monitor the hydrolysis of rhodamine 6G. Luminescence 27, 482–488. https://doi.org/10.1002/bio.1379

Zouzelka, R., Rathousky, J., 2017. Photocatalytic abatement of NO_x pollutants in the air using commercial functional coating with porous morphology. Appl. Catal. B Environ. 217, 466–476. https://doi.org/10.1016/j.apcatb.2017.06.009